

ELSEVIER

Tectonophysics 282 (1997) 1–38

TECTONOPHYSICS

## Paleostress reconstructions and geodynamics of the Baikal region, Central Asia, Part 2. Cenozoic rifting

Damien Delvaux <sup>a,\*</sup>, Rikkert Moeys <sup>b</sup>, Gerco Stapel <sup>b</sup>, Carole Petit <sup>c</sup>, Kirill Levi <sup>d</sup>,  
Andrei Miroshnichenko <sup>d</sup>, Valery Ruzhich <sup>d</sup>, Volodia San'kov <sup>d</sup>

<sup>a</sup> Royal Museum for Central Africa, Department of Geology–Mineralogy, B-3080 Tervuren, Belgium

<sup>b</sup> Vrije Universiteit Amsterdam, De Boelelaan 1085, 1081 HV Amsterdam, The Netherlands

<sup>c</sup> UMR 125 Géosciences Azur, Observatoire Océanologique, B.P. 48, F-06230 Villefranche-sur-Mer, France

<sup>d</sup> Institute of the Earth's Crust, SB, RAS, Lermontov st. 128, 664033 Irkutsk, Russia

Received 1 February 1996; accepted 1 October 1996

### Abstract

Investigations on the kinematics of rift opening and the associated stress field present a renewed interest since it has recently been shown that the control of the origin and evolution of sedimentary basins depends to a large extent on the interplay between lithospheric strength and applied stresses. It appears that changes of stress field with time are an important factor that either controls or results from the rifting process. The object of this paper is to study the changes of fault kinematics and paleostress field with time in the Baikal Rift System during the Cenozoic. Reduced paleostress tensors were determined by inversion from fault-slip data measured in the central part of the rift and its southwestern termination, between 1991 and 1995. Results show that the stress field varies as well in time as in space. Two major paleostress stages are determined, corresponding broadly to the classical stages of rift evolution: Late Oligocene–Early Pliocene and Late Pliocene–Quaternary. The first paleostress stage is related to the rift initiation and the second to the major stage of rift development. Similarities between the recent paleostress field and the present-day stress field inverted from focal mechanisms indicate that the second paleostress stage is still active. Therefore, we propose to use ‘proto rift’ for the Late Oligocene–Early Pliocene stage and ‘active rift’ for the Late Pliocene–Quaternary stage of rift development. During the ‘proto rift’ stage, the stress field was characterized by a compressional to strike-slip regime. A progressive change from transpression to transtension is suspected for the central part of the rift (Baikal and Barguzin basins) during this period. In the western termination of the rift (Sayan Massif, Tunka depression), a strongly compressional stress field with oblique thrusting kinematics is well constrained in the Late Miocene–Early Pliocene interval. The ‘active rift’ stage was initiated by a marked change in fault kinematics and stress regime in the Late Pliocene. In the central part of the rift, the stress regime changed into pure extension, while in the southwestern extremity, it changed into pure strike-slip. Fault kinematics suggests that rifting was initiated by an extrusion mechanism due to the interaction of far-field compressional stress on a mechanically heterogeneous crust, with the southwards-pointing wedge of the Siberian Craton acting as a passive indenter. The Cenozoic time–space evolution of the stress field is believed to reflect the increasing influence of locally generated buoyancy extensional stresses associated with density anomalies of the lithosphere, on intraplate stresses generated by the India–Eurasia convergence and the West-Pacific subduction.

**Keywords:** Siberia; Baikal Rift Zone; Cenozoic; structural geology; tectonophysics; paleostress

\* Corresponding author. Tel.: +32 2 7695 420; fax: +32 2 7695 432; e-mail: ddelvaux@africamuseum.be

## 1. Introduction

In the last decades, substantial progress has been made in the understanding of the thermomechanical and isostatic processes in the lithosphere related to sedimentary basin formation (Braun and Beaumont, 1989). It appears that the control of the origin and evolution of sedimentary basins depends mainly to the interplay between lithospheric strength (rheology) and the applied stresses (Zoback et al., 1993). The subsidence, architecture and stratigraphy of both extensional and compressional basins are significantly controlled by the changes in plate tectonic regimes and associated stress field (Cloetingh and Kooi, 1992; Kooi and Cloetingh, 1992). At the onset of rifting, the stress field in rift zones is generally dominated by intraplate stresses generated by external, often compressional plate-driving forces (Ziegler, 1996). In the course of rifting, local buoyancy extensional forces can be generated by density anomalies due to crustal thickening or lithospheric thinning. These extensional stresses may be comparable or even exceed the intraplate stress field (Sonder, 1990; Richardson, 1992; Zoback, 1992; Engelder, 1993).

After the initial collision of India with Eurasia in the Paleocene–Early Eocene, India continued to converge northwards with a reduced velocity and was progressively indented into Eurasia (Patriat and Achache, 1984). This post-collisional convergence induced strong deformation in Central and South-east Asia (Molnar and Tapponnier, 1975; Cobbold and Davy, 1988). A large part of the Asian plate is affected by compressive stresses, mainly generated by the India–Eurasia convergence, but also constrained by the Pacific/Asia subduction (Tapponnier and Molnar, 1979; Zonenshain and Savostin, 1981; Zhonghuai et al., 1992; Zoback, 1992). The northwestern boundary between stable Eurasia (Kazakhstan and Siberian plates) and South-East Asia is formed by a broad zone of tectonic deformation, including the Pamir, Tian-Shan, Altai and Sayan mountains, the Baikal Rift System, the Stanovoy belt and Okhotsk Sea (Tapponnier and Molnar, 1979; Parfënoy et al., 1987; Cobbold and Davy, 1988; Worrall et al., 1996). To the west, it is bounded by the Pacific subduction.

According to Molnar and Tapponnier (1975), the India–Eurasia convergence is a likely mechanism

which could explain the Cenozoic tectonics of Central Asia, including the Baikal Rift System. For Logatchev and Zorin (1987, 1992), Logatchev (1993) and Windley and Allen (1993), the development of the Baikal Rift System and adjacent region in North Mongolia is mainly related to the intrusion of a major asthenospheric diapir. However, for Kieslev and Popov (1992), Baljinyam et al. (1993) and Delvaux and Klerkx (1994), the tectonic evolution of Baikal and North Mongolia is a combination of these two processes.

The present-day stress field in the Baikal Rift System and adjacent regions has been first established by statistical analysis of P and T axes of earthquake focal mechanisms (Zonenshain and Savostin, 1981; Solonenko, 1993; Solonenko et al., 1997). The first stress inversion of focal mechanisms was done for the North Muya region in the northwestern branch of the rift (Déverchère et al., 1993). A revised database of 332 focal mechanisms has been used by Petit et al. (1996) to compute stress tensors for a series of fifteen sub-regions in the whole Baikal Rift System. Together with the data of adjacent regions, the Baikal Rift System appears as an anomalous region of active extensional tectonics in the middle of the Eurasian plate, dominantly submitted to compression. Petit et al. (1996) concluded that the Baikal Rift is the result of the interaction between plate-scale stress field, inherited lithospheric structures and the geometry of the Siberian Craton. However, several questions remain unsolved: how does the stress field evolved with time during the rifting process? Was the stress field stable during all the rifting history? In case of stress change, when was the present-day stress field established and what was the stress field at the beginning of rifting? To what extent is the modification of stress field with time related to the evolution of the rifting process itself or to the modification of external (plate-scale) stress field in the course of rifting? The investigation of the stress field evolution with time can also contribute to the question regarding the origin of the lithospheric anomalies and the related buoyancy stresses, and hence to the long debate between active and passive causes of rifting.

Various kinematic models were already proposed to explain the opening of the Baikal Rift System. Balla et al. (1991) proposed an oblique opening, controlled by sinistral strike-slip movement along E–W

striking fault systems. Lukina (1988) and Sherman (1992) suggest that the NE-trending Lake Baikal depression opens as a giant tension gash by normal faulting, between the two E–W-trending segments with sinistral strike-slip movements. From the analysis of a limited number of teleseisms, Doser (1991a,b) shows that about one third of the earthquakes studied show a strike-slip mechanism. From the morphological analysis of Holocene scarps and offset river fans in the northeastern segment of the Baikal Rift System, Houdry (1994) and Houdry et al. (1994) suggest that the Holocene extension was oblique to the major rift fault trend, with a WNW–ESE direction of movement. They show that the general context is sinistral-transensional, and the pattern of en echelon normal faults is determined by the reactivation of inherited basement faults. They also suggest that the general en-echelon pattern of rhomb-shape basins of the northeastern rift segment can be explained by the reactivation of an existing network of older fault system. They believe that this part of the rift cannot be interpreted as a system of pull-apart basins developing along a sinistral transform, as proposed by Lukina (1988) and Sherman (1992).

The presence of late Cenozoic compressional tectonics with thrusting kinematics in the southwestern extremity of the Baikal Rift System was first shown by Ruzhich et al. (1972), thanks to the discovery of a 10–14 Ma dyke deformed by thrusting in the Tunka Range. More recently, Rasskazov (1990) demonstrated the presence of a reverse fault with more than 300 m of throw, affecting 2.6 Ma basalts in the Oka plateau, north of the Darkhat basin.

The Cenozoic stress field in the Baikal Rift System was first investigated by Sherman and Dneprovski (1989) and Sherman (1992). They show that the opening of Lake Baikal is related to a general stress field with NE–SW horizontal principal compression ( $S_{Hmax}$ ) and NW–SE principal extension ( $S_{Hmin}$ ). However, they reconstructed the stress field in terms of geometrical axes and not in terms of reduced stress tensors. They used only joint sets, following the technique of Nikolaev (1977). They underline the geographical variation of stress field and fault kinematics from the central part of the rift system towards both extremities. They implicitly assume a stable kinematic regime during the entire rifting process, despite several observations suggest-

ing temporal variations of stress regime (Ruzhich et al., 1972; Sherman et al., 1984; Rasskazov, 1985, 1993; San'kov et al., 1991).

This paper aims at investigating the spatial and temporal variations of stress field in the Baikal Rift System during the Cenozoic, using fault-slip data. It intends to precise the timing of the two rift phases evidenced by Logatchev and Florensov (1978) and Logatchev and Zorin (1987), and to determine their characteristics in terms of stress evolution. Paleostress tensors are reconstructed using a standard technique of inversion of fault-slip data. Data on fault planes and slip lines were collected in the course of five field expeditions in the western and central parts of the Baikal Rift from 1991 to 1995. The microstructural data concerning pre-rift tectonic events in the Paleozoic and Mesozoic are presented and discussed in Delvaux et al. (1995).

## 2. Tectonic setting

The Baikal Rift System is located at the southern margin of the Siberian Platform, along the suture zone with the Sayan–Baikal Caledonian fold belt of Central Asia (Fig. 1). This marginal zone has been subjected to repeated tectonic movements and major reactivations during the Late Proterozoic, Paleozoic and Mesozoic (Logatchev and Zorin, 1992; Ermikov, 1994; Melnikov et al., 1994; Delvaux et al., 1995). The southern margin of the Siberian Craton displays a characteristic southwards-pointing wedge, the Angara–Lena Platform. Towards the northeast, the Vitim Embayment separates the Angara–Lena Platform from the Aldan Shield. The deepest rift basins, corresponding to the Lake Baikal depression, are largely superimposed on the suture zone along the southeastern side of the platform (Fig. 2). To the southwest, the platform is separated from the East Sayan Massif, by the Main Sayan fault zone. The northeastern part of the rift zone is splayed in several subparallel basins in the Vitim Embayment. The structural evolution of the Baikal Rift System has been controlled to a large extent by the reactivation of ancient tectonic structures (Zamaraev and Ruzhich, 1978).

The elevated area related to the Baikal Rift System (Figs. 2 and 3) is generally described as the ‘Baikal–Sayan arched uplift’ (Logatchev and Flo-

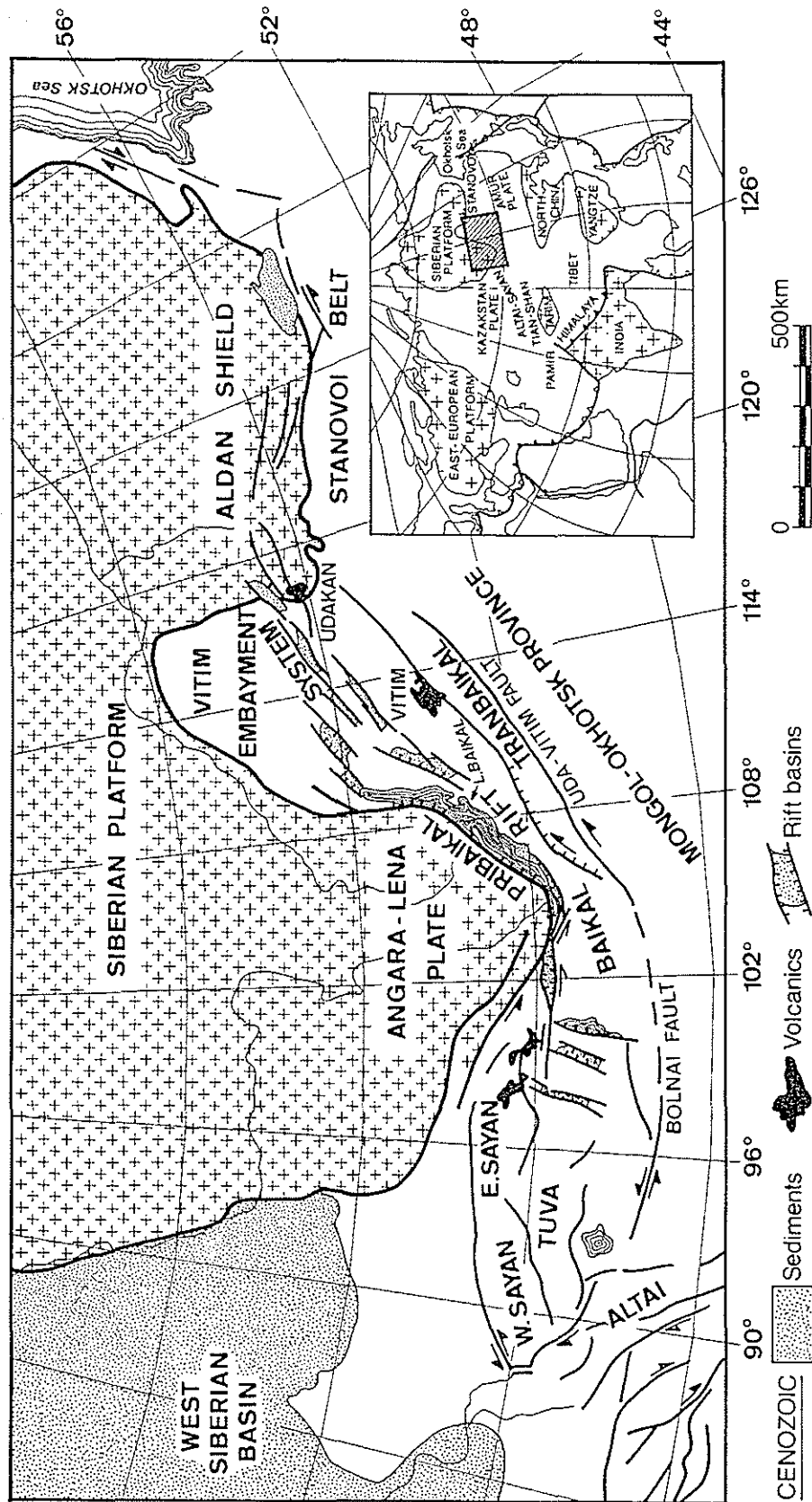


Fig. 1. Tectonic setting of the Baikal region in Central Asia.

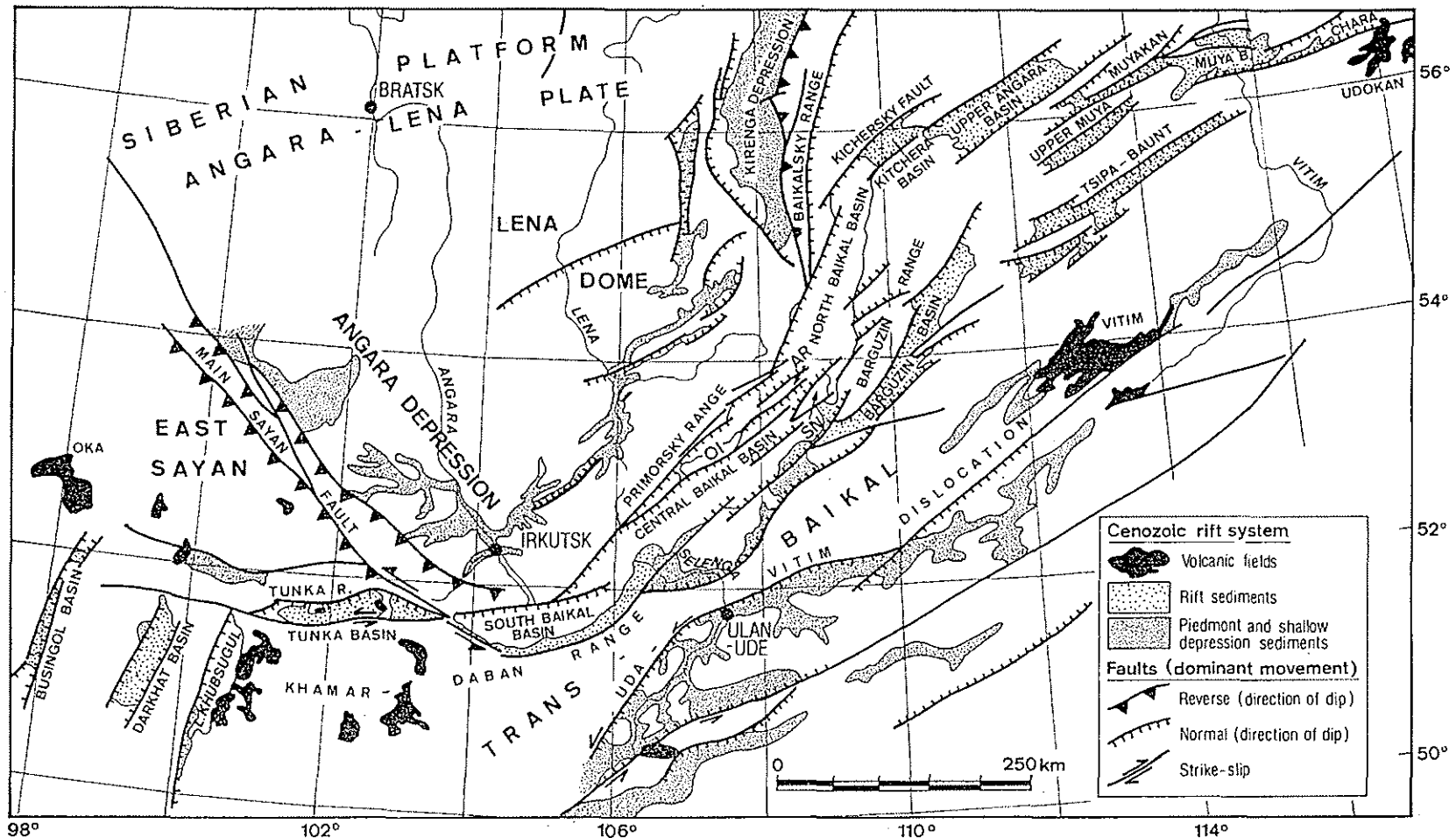


Fig. 2. Structural map of the Baikal Rift Systems with major rift basins, Quaternary shallow depressions and Cenozoic faults (compiled from Levi et al., 1982).

## Baikal area: Digital Terrain Model

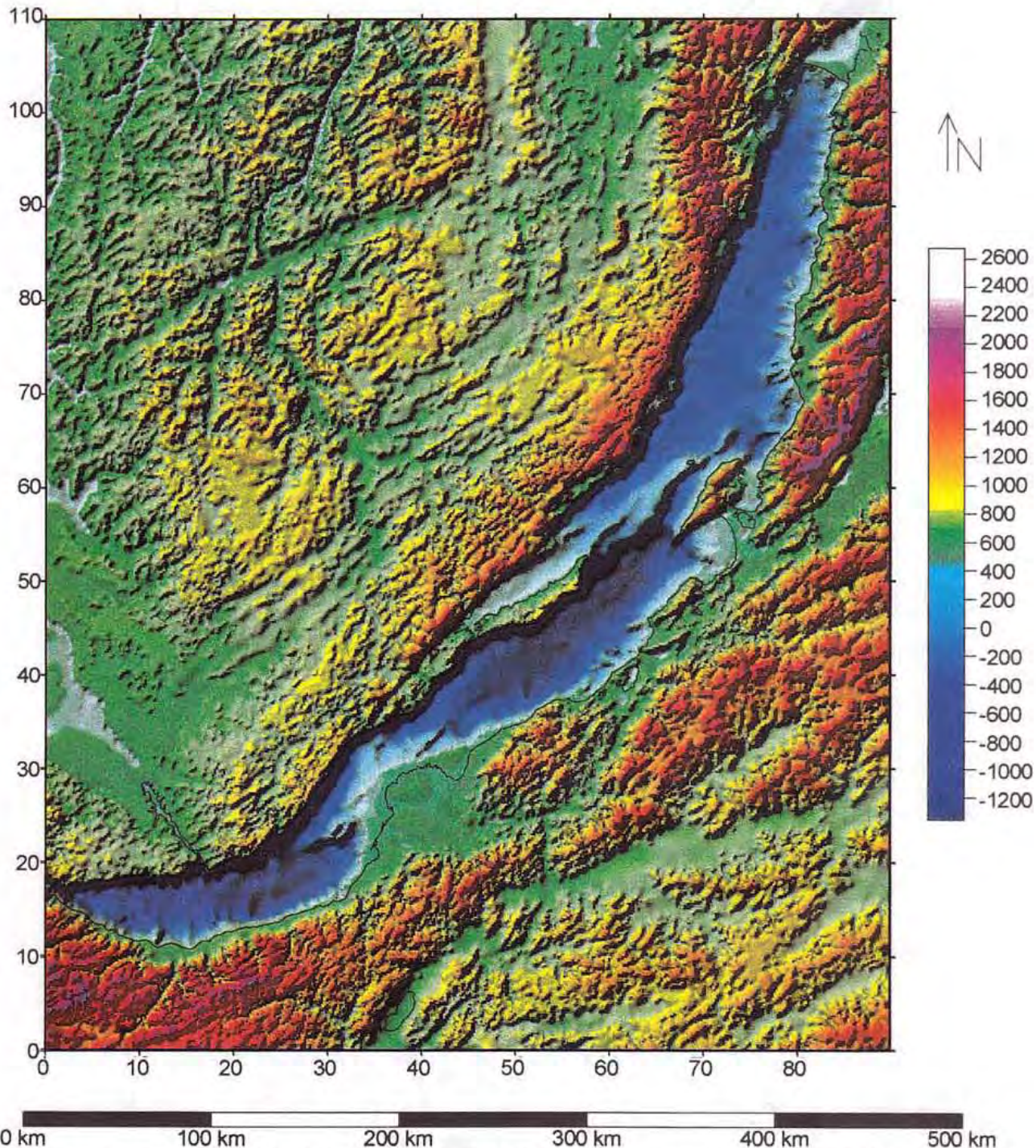


Fig. 3. Digital Terrain Model (DTM) of Lake Baikal depression and adjacent areas processed by Microsoft SURFER. Colour altitude map superposed on a shaded relief map with artificial illumination from the northwest. Altitude of lake level is 456 m. Topographic height contour digitised from 1/500,000 and 1/1,000,000 touristic maps. Lake bathymetry digitized from 1/200,000 bathymetric map. See Fig. 2 for reference to geographical names and structural elements.

rensov, 1978). More precisely, the central part of the rift is relatively depressed (Angara–Selenga saddle, 900–1400 m high), between two strongly uplifted areas: the East Sayan Massif to the southwest (2000–3250 m) and the North Baikal uplift to the northeast (2650–2800 m). The surface of the lake is 456 m a.s.l. and the lake is up to 1640 m deep. Southeast of the rift zone, the Transbaikal area is characterized by a series of short-wavelength (30 km) shallow sedimentary depressions and mountain ranges (900 to 1600 m high) which reactivate older Mesozoic structures (Ermikov, 1994). The Baikal basin is flanked to the northwest by the Primorsky–Baikalsky rift shoulder (1000–2500 m high, 50 km wide). The margin of Angara–Lena Platform lies at 400–800 m a.s.l, but its central part rises up to 1500 m high and forms the Lena Dome. A system of shallow sedimentary basins develop along the rim of the Angara–Lena Platform, in the depressed area between the Lena Dome and the mountain ranges bordering the rift (North Baikal uplift, the Primorsky–Baikalsky rift shoulder and East Sayan Massif).

The central part of the rift is occupied by the Barguzin depression and the Lake Baikal depression. The latter is subdivided into the South, Central and North Baikal basins (Figs. 2 and 3). The Central Baikal basin is separated from the South Baikal basin by the Posolskaya bank and from the North Baikal basin by the underwater Academician Ridge. The northeastern continuation of the rift system is marked by a series of rhomb-shaped en-echelon grabens, including the Upper Angara, Muya, North Muya, Chara and Toka basins (see Logatchev, 1993 for the location of the last two). The southwestern extremity of the rift system is occupied by the E–W-trending Tunka depression and a system of NS-trending depressions in North Mongolia (Lake Khubsugul, Darkhat and Busingol basins). The Tunka depression lies in the western continuation of the South Baikal basin (Fig. 4), but in a very different context. It developed between the Tunka Range front and the South Tunka sinistral strike-slip fault. It presently consists of five isolated basins, separated by uplifted blocks (Sherman and Ruzhich, 1973).

The upper mantle below the Baikal Rift System and adjacent areas shows anomalous geophysical properties (Zorin et al., 1989; Diament and Kogan, 1990; Ruppel et al., 1993). Teleseismic investigation confirms the presence of a broad asthenospheric

upwarp beneath the central part of the Baikal Rift System and its shoulders (Gao et al., 1994a). The same experiment also reveals a seismic anisotropy in the mantle, suggesting that the asthenospheric upwarp beneath Central Baikal is likely to be caused by horizontal mantle flow in a NW–SE direction, normal to the rift axis (Gao et al., 1994b). Gravity modelling (Burov et al., 1994) and seismic velocity inversion (Petit and Déverchère, 1995) show that the crust in the northeastern part of the Baikal Rift System is unbalanced and affected by a strong mechanical discontinuity separating two blocks of different thickness. This structure is interpreted as inherited from an earlier tectonic event which destabilized the crust before the present stage of extension. The kinematics of extension of the Baikal Rift appears to be controlled by a strong elastic lithosphere with significant brittle deformation of the upper crust (Van der Beek, 1997).

### 3. Structural, stratigraphic and volcanic evolution

In this section, we present a brief review of recently published data on the structural, stratigraphic and volcanic evolution of rifting (Fig. 5), some of which are still poorly known from the international community. A good synthesis of the tectonic history of rifting is also necessary for the interpretation of the results of paleostress analysis, as discussed later.

The area of the Baikal Rift System underwent intense uplift and denudation in the *Late Jurassic–Early Cretaceous*, in relation to the closure of the Mongol–Okhotsk ocean in Central Mongolia (Delvaux et al., 1995; Van der Beek et al., 1996). In the *Late Cretaceous–Paleogene*, the whole region covering the Altai, Mongolia and Baikal areas was in stable tectonic conditions under a warm and humid climate, allowing the development of a prominent planation surface with deeply weathered kaolinite–gibbsite and laterite–bauxite horizons (Devyatkin, 1975, 1981; Kashik and Mazilov, 1994).

It is unclear when real Early Tertiary lacustrine sedimentation started in the Baikal area, but fine clays and sediments derived from the weathering horizon and dated as Paleocene–Eocene by palynology have been reported at various places (Kashik and Mazilov, 1994). The presence of Paleocene to Early

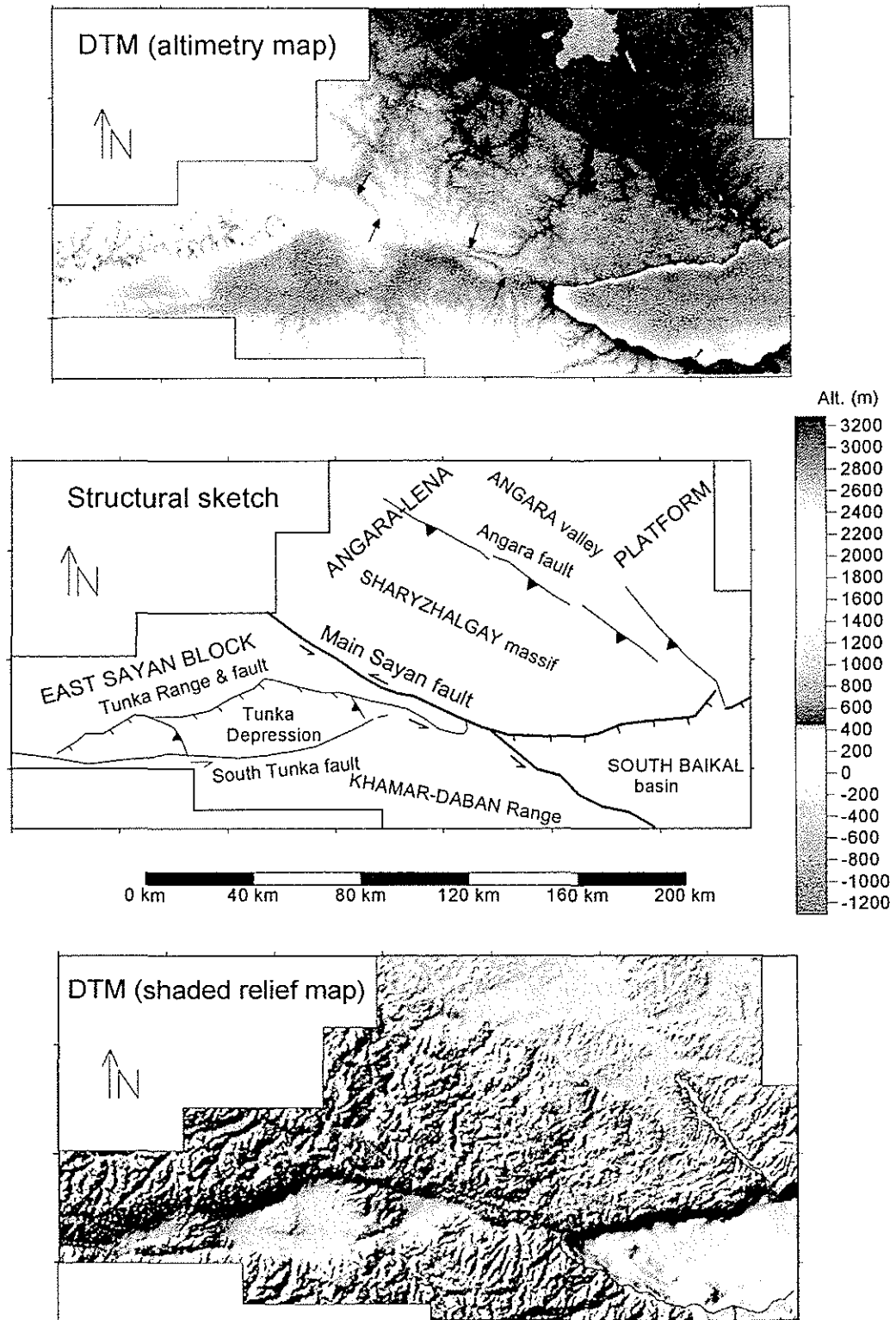


Fig. 4. Digital Terrain Model (DTM) of the Tunka depression and the western extremity of the Lake Baikal basin, processed by Microsoft SURFER. Altitude map with colour in function of altitude or bathymetry with reference to sea level (lake level is 456 m a.s.l.). Shaded relief map with artificial illumination from the northwest. Topographic height contour digitised from 1/200,000 topographic maps of the East-Siberian aero-geodesic office of the National Geodesic Committee of the former USSR (1990), and processed by SURFER. Offset valleys along the Main Sayan fault are indicated by small black arrows.

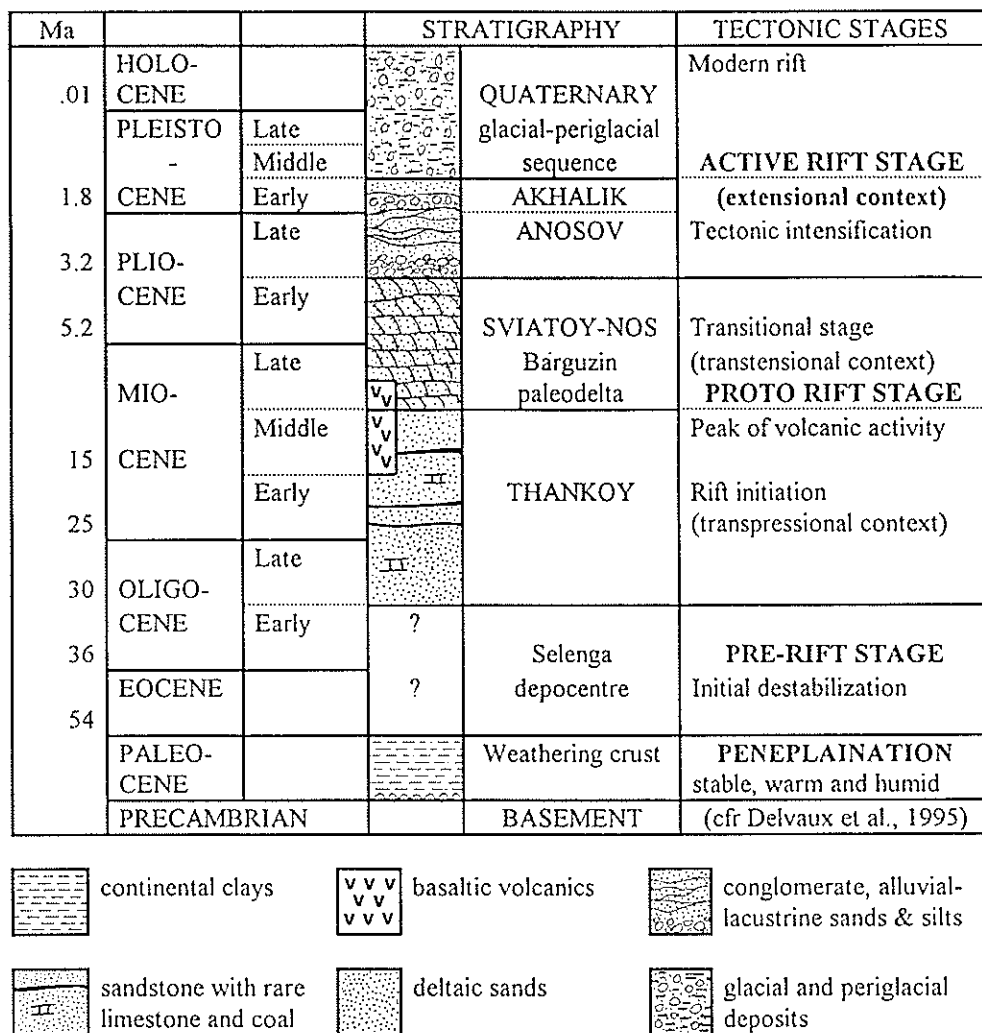


Fig. 5. Stratigraphic overview of the Baikal Rift System, with the major tectonic events.

Eocene sediments in the area of the Selenga delta is inferred from borehole results (Logatchev, 1993). The oldest dated deposits in the Tunka depression are Oligocene series (palynology by Mazilov et al., 1993). Moderate volcanism in Transbaikal in the Late Cretaceous–Paleogene period is known along a relatively linear belt including the Tunka area, Khमार Daban Ridge and the Vitim plateau (Bagdasaryan et al., 1981; Eudrichinsky, 1991; Rasskazov, 1994).

### 3.1. 'Slow rifting'–'fast rifting' model

The initiation of rifting in the Baikal basin, marked by fault-controlled uplift, sedimentation and volcanism, occurred in the Late Oligocene (Lo-

gatchev, 1993; Mazilov et al., 1993; Rasskazov, 1994). The thickness of Cenozoic sediments reaches 8–10 km in the South and Central Baikal basins and no more than 4.5 km in the North Baikal basin (Hutchinson et al., 1992; Scholz et al., 1993). In the Miocene–Early Pliocene, the Baikal rift is composed of independent and relatively deep long-lived lakes (Popova et al., 1989). This corresponds to the 'slow rifting' stage defined by Logatchev and Florensov (1978). In the Late Pliocene, a major acceleration of tectonic movements occurred. Fast basin subsidence took place in the Baikal Rift System in a dominantly extensional context and the Khubsugul, Busingol and Darkhat depressions started to develop (Baljinyam et al., 1993; Logatchev, 1993). This stage is described as the 'fast rifting' stage by Logatchev

and Florensov (1978). The classical two-stage rifting model can be further refined and the following stages of development are recognized.

### 3.2. Late Oligocene–Middle Miocene rift initiation (30–8 Ma)

In the Late Oligocene–Middle Miocene, lacustrine basins of several tens to hundred metres deep are evidenced in the Tunka, South Baikal and Central Baikal depressions. They were framed by mountain ranges not higher than a few hundred metres above the water level (Popova et al., 1989). Shallow-water depressions are also present in the northern extremity of the North Baikal basin and in the Barguzin basin (Popova et al., 1989), the latter from the Middle Miocene only (Zorin et al., 1989). Until Middle Miocene, the Central Baikal basin was limited to the north by a continuous land barrier comprising Olkhon Island, the underwater Academician Ridge, Ushkany Island, the Sviatoy Nos Peninsula and the Barguzin Ridge (Kazmin et al., 1995). The South and Central basins were highly asymmetric and subsidence was controlled by south- to southeast-dipping faults along the northwestern border (Zonenshain et al., 1993).

The Late Oligocene–Middle Miocene sediments are described as the *Thankoy formation*. They include sandstones, siltstones, clays and rare limestones. They are of lacustrine, swampy and fluvial facies with coal seams (Artyushkov et al., 1990; Kashik and Mazilov, 1994). The *Thankoy formation* corresponds broadly to the first seismostratigraphic unit recognized by Hutchinson et al. (1992) and Scholz et al. (1993) on multichannel seismic profiles, and present only in the South and Central Baikal basins.

Episodic volcanic activity occurred since 29 Ma, but the major volume of Cenozoic lava was erupted between 14 and 8 Ma on the uplifted ranges bordering the Baikal Rift (Khamar–Daban and Vitim) and in the Tunka depression (Rasskazov, 1993, 1994). Relief differentiation in the East Sayan, Khamar Daban, Vitim and Udokan areas is evidenced in this period by the presence of paleovalleys, 400–500 m deep, preserved beneath Mid-Miocene basalts (Logatchev, 1993; Rasskazov, 1994).

### 3.3. Late Miocene–Early Pliocene transition stage (8–3 Ma)

In the Late Miocene, a first important modification of the basins architecture and biota occurred, due to changes in tectonic and climatic regimes. Volcanic activity dropped sharply between 8 and 5 Ma, while the uplift was intensified. The surface and depth of the South and Central Baikal basins increased. The land barrier between the Central and the North Baikal basins was progressively disrupted, but deep lakes are still absent in North Baikal (Popova et al., 1989). The South and Central basins evolved into more symmetrical grabens, bounded by faults with normal component of movement on both sides (Kazmin et al., 1995).

Multichannel seismics, coupled with direct underwater observations and palynological dating of samples taken by manned submersibles showed that subsidence of the Academician Ridge and horst-and-graben structure between Ushkany Island and Sviatoy Nos Peninsula were initiated in the Late Miocene (Zonenshain et al., 1993). The disruption of this former land barrier was caused by faulting with a marked normal component (Kazmin et al., 1995). This allowed the transportation of clastic material from the Barguzin River to the southern margin of the North Baikal basin. The sediments of the Barguzin paleodelta (*Sviatoy Nos formation*) lay directly on the basement floor of the Academician Ridge and are dated as Late Miocene–Early Pliocene according to palynology (Kazmin et al., 1995). Similar underwater investigation between the South- and Central Baikal basins also evidenced Early Pliocene normal faulting in the Posolskaya bank (Bogdanov and Zonenshain, 1991).

### 3.4. Late Pliocene–Early Pleistocene tectonic intensification (3–1 Ma)

In the Late Pliocene–Early Pleistocene, significant reorganisation of the lake system occurred, due to rapid acceleration of tectonic processes, general uplift and climate cooling (Popova et al., 1989). It resulted in contraction and shallowing of the large lakes. By the end of the Pliocene, only shallow lakes remained in the Tunka basin, limited and relatively deep lakes existed in the South and Central

Baikal basins and shallow lakes occupied most of the northern basin (Popova et al., 1989). The disruption of the land barrier in symmetrical horsts and grabens between the Central and South Baikal basins is now complete (Kazmin et al., 1995), forming a typical accommodation zone as those described for the East-African Rift (Morley et al., 1990). During this period, the Primorsky rift shoulder was still not well developed, allowing the water to flow out of Lake Baikal by the Buguldeyka–Manzurka–Lena river system (Mats, 1993). Similarly, the Lena Dome in the center of the Angara–Lena Platform also developed relatively recently, as shown by the deep incision of the Lena River in the middle of the dome.

The Late Pliocene and Early Pleistocene deposits, respectively defined as *Anosov* and *Akhalik suites*, are composed of conglomerates, gravelstones, sandstones and siltstones of lacustrine, fluvial and alluvial facies (Kashik and Mazilov, 1994). In the Academician Ridge area, Zonenshain et al. (1993) and Kazmin et al. (1995) show that this unit corresponds to slightly deformed, rapidly accumulating sediments covering the Late Miocene–Early Pliocene deltaic sequence of the Sviatoy Nos formation.

In the South and Central Baikal basins, the Russian seismic profiles show that the Thankoy formation is unconformably overlain by the *Anosov* and *Akhalik suites* (Nikolaev, 1990). These two suites are well stratified and deformed in many places: folded and thrust in the South Baikal basin, faulted in the Selenga delta and affected by flower structures in both the South and Central Baikal basins (Levi et al., 1998). The last seismostratigraphic unit (middle-Late Pleistocene sediments of glacial and deltaic facies) lies unconformably and undisturbed above the folded structure of the South Baikal basin. From this description, we can infer the existence of a compressive stage in the southern basin during the Late Pliocene–Early Pleistocene interval.

### 3.5. Middle Pleistocene–Holocene modern rift stage (1–0 Ma)

In the middle Pleistocene, a new acceleration of vertical tectonic movements resulted in the constitution of the present integrally deep Baikal depression (Popova et al., 1989). An increasing rate of uplift of the western rift shoulder led to the blockage of the

former Buguldeyka–Manzurka–Lena outlet of Lake Baikal 0.7–0.8 Ma ago. This caused a rise in lake level, and the formation of a new outlet channel, via the Irkut River to the Yenisey (Popova et al., 1989). In the Late Pleistocene, at about 0.1 Ma, subsidence of the northern shoulder of the South Baikal basin resulted in a redirection of the outlet to the upper part of the Angara river (Mats, 1993).

The acceleration of the rift shoulder uplift and basin subsidence occurred together with an intensification of extensional tectonics. The opening of the Small Sea between Olkhon Island and the Primorsky Range, due to normal faulting along the Primorsky fault, can be as young as 1 Ma (Agar and Klitgord, 1995). In general, the rift system reaches the highest level of symmetry, with development of normal faults on both sides of the grabens (Kazmin et al., 1995). In East Sayan, Holocene fault scarps of up to 30 m high developed at the foot of the Tunka Range front (McCalpin and Khromovskikh, 1995).

In summary, the Baikal Rift System has a long and complex history, characterized by highly changing tectonic activity. A major change of tectonic regime and acceleration of vertical movements occurred in the Late Pliocene, about 3 Ma ago. The last tectonic stage is only 1 Ma old. This implies that the present-day tectonic regime reconstructed from Holocene fault scarps (e.g., Houdry, 1994) and earthquake focal mechanisms (Petit et al., 1996) cannot be extrapolated back over a long period. Therefore it is also necessary to investigate the fault kinematics and stress field evolution with time.

## 4. Stress field reconstruction

We present here the method used for reconstruction of reduced stress tensors from fault slip data. We introduce also a quality ranking and an index to express numerically the stress regime. The results of paleostress determination are presented and paleostress stages are defined. Finally, we discuss the regional stress field evolution with time.

### 4.1. Paleostress inversion from fault slip data

Reduced paleostress tensor determinations and separation of fault populations were made by a numerical method, according to the standard proce-

dures (Angelier, 1991, 1994; Dunne and Hancock, 1994). The inversion is based on the assumption of Bott (1959) that slip on a plane occurs in the direction of the maximum resolved shear stress. The apparent slip direction on the fault plane is inferred from frictional grooves or slickenlines. Fault and joint data were inverted to obtain the four parameters of the reduced stress tensor: the principal stress axes  $\sigma_1$  (maximum compression),  $\sigma_2$  (intermediate compression) and  $\sigma_3$  (minimum compression) and the ratio of principal stress differences  $R = (\sigma_2 - \sigma_3)/(\sigma_1 - \sigma_3)$ . The latter defines the shape of the stress ellipsoid. Several definitions of the stress ratio are found in the literature (e.g., Carey-Gailhardis and Mercier, 1987; Angelier, 1994). The one used here is the equivalent of the  $\phi$  ratio of Angelier (1994). The two additional parameters of the full stress tensor are the ratio of extreme principal stress magnitudes ( $\sigma_3/\sigma_1$ ) and the lithostatic load, but these cannot be determined from fault data only. The first four parameters are determined by using successively an improved version of the right dihedral method of Angelier and Mechler (1977), and a four-dimensional numeric rotational optimisation method, using the TENSOR program (Delvaux, 1993). This program allows to optimise a wide variety of functions, independently or combined: minimisation of deviation angles ( $\alpha$ ) between observed and predicted slips on fault planes; maximisation of shear stress magnitude ( $\sigma_t$ ) on fault planes and shear joints; minimisation of normal stress magnitude ( $\sigma_n$ ) on extensional joints (tension veins . . . ) and maximisation of normal stress magnitude ( $\sigma_n$ ) on compressional joints (cleavage, stylolites . . . ). Most stress tensors were computed using a composite function, with simultaneous minimisation of deviation angles  $\alpha$  for fault planes, maximisation of  $\sigma_t$  on fault planes and shear joints and minimisation of  $\sigma_n$  on extension joints. Critical considerations on the accuracy of stress inversion methods are given in Dupin et al. (1993) and Pollard et al. (1993). They concluded that uncertainties in stress tensor determination due to geological and mechanical factors generally fall in the range of measurement errors.

A quality rank criterion, ranging from A (very good) to D (poor), is determined as in Table 1. It depends on the number of data used for the stress inversion ( $n$ ), the ratio of used data versus the total

Table 1

Quality ranking criteria for stress tensor determination by inversion of fault-slip data

Qual.	Description	Accuracy parameter
A	good	>1.5
B	medium	0.5–1.5
C	poor	0.3–0.5
D	not reliable	<0.3

Accuracy parameter is  $n \times (n/n_T)/\alpha$  with  $n$  the number of data explained by the tensor solution;  $n/n_T$  the ratio of explained data in the total population;  $\alpha$  mean slip deviation for all faults used.

fault population ( $n/n_T$ ), and the average slip deviation between observed and predicted slips ( $\alpha$ ). The tensors from sites with polyphase sets of fault data will therefore have lower ranks than single-phase sites, for the same amount of data. When possible, these sites were oversampled, to avoid a quality degradation of the computed tensors. While sites with a single set of fault-slip data have generally 10 to 50 measurements with a mean number of 20–30, polyphase sets may have 40 to 100 measurements. Those polyphase sites are shown in Appendix A by an index mentioning to which phase the second (or third) set belongs: o = pre rift phase, p = proto rift phase, a = active rift phase. When using other data then fault planes with slip lines (e.g., pairs of conjugated joints), the quality rank is lowered by one level, to take into account additional uncertainties involved in the stress inversion.

#### 4.2. Stress regime and stress field characterisation

In this article, we use the term ‘stress regime’ to define the type of stress tensor. The stress regime is determined by the nature of the vertical stress axes: extensional when  $\sigma_1$  is vertical, strike-slip when  $\sigma_2$  is vertical, and compressional when  $\sigma_3$  is vertical. Inside these three major types, the stress regimes also vary in function of the stress ratio  $R$  (Fig. 6): radial extension ( $\sigma_1$  vertical,  $0 < R < 0.25$ ), pure extension ( $\sigma_1$  vertical,  $0.25 < R < 0.75$ ), transtension ( $\sigma_1$  vertical,  $0.75 < R < 1$  or  $\sigma_2$  vertical,  $1 > R > 0.75$ ), pure strike-slip ( $\sigma_2$  vertical,  $0.75 > R > 0.25$ ), transpression ( $\sigma_2$  vertical,  $0.25 > R > 0$  or  $\sigma_3$  vertical,  $0 < R < 0.25$ ), pure compression ( $\sigma_3$  vertical,  $0.25 < R < 0.75$ ) and radial compression ( $\sigma_1$  vertical,  $0.75 < R < 1$ ). The

Stress tensor type	EXTENSIVE				STRIKE-SLIP				COMPRESSIVE				
Stress symbols													
Stress ratio R	0.00	0.25	0.50	0.75	1.00	0.75	0.5	0.25	0.00	0.25	0.50	0.75	1.00
Stress regime	Radial EXTENSIVE		Pure EXTENSIVE		TRANS-TENSIVE	Pure STRIKE-SLIP		TRANS-PRESSIVE	Pure COMPRESSIVE		Radial COMPRESSIVE		
Stress index R'	0.00	0.25	0.50	0.75	1.00	1.25	1.50	1.75	2.00	2.25	2.50	2.75	3.00
Determination of R'	R' = R				R' = 2 - R				R' = 2 + R				

Fig. 6. Illustration of the meaning of stress regime index  $R'$  versus stress ratio  $R$  and orientation of the principal axes of the stress ellipsoid. Stress symbols with horizontal stress axes ( $S_{Hmax}$  and  $S_{Hmin}$ ), as a function of the stress ratio  $R$ . Their length and colour symbolise the horizontal deviatoric stress magnitude, relative to the isotropic stress ( $\sigma_i$ ). White outward arrows: extensional deviatoric stress ( $<\sigma_i$ ). Black inwards arrows: compressional deviatoric stress ( $>\sigma_i$ ). The vertical stress ( $\sigma_v$ ) is symbolised by a solid circle for extensional regimes ( $\sigma_1 = \sigma_v$ ), a dot for strike-slip regimes ( $\sigma_2 = \sigma_v$ ) or an open circle for compressional regimes ( $\sigma_3 = \sigma_v$ ).

type of stress regime can be expressed numerically using an index  $R'$ , ranging from 0.0 to 3.0 and defined as follows (Fig. 6):

- $R' = R$  when  $\sigma_1$  is vertical (extensional stress regime)  
 $R' = 2 - R$  when  $\sigma_2$  is vertical (strike-slip stress regime)  
 $R' = 2 + R$  when  $\sigma_3$  is vertical (compressional stress regime)

The index  $R'$  defines the stress regime completely and is convenient for computing the mean regional stress regime from a series of individual stress tensors in a given area.

On structural maps, the stress tensors are displayed with the orientation of both horizontal principal stress ( $S_{Hmax}$ ) and horizontal minimum stress axes ( $S_{Hmin}$ ), as recommended by Guiraud et al. (1989) and shown in Fig. 6.

After the inversion, the reduced stress tensors are grouped into regional paleostress stages in function of stratigraphic constraints, stress regime and orientation of principal stress axes. The relative timing is estimated from cross-cutting relationships in fault-slip data and the relation of the observed sites with macrostructures. The time range for these paleostress stages is estimated in function of the stratigraphic constraints and of the general morpho-tectonic evo-

lution of the Baikal Rift System. In this article, 'stress field' is defined as the regional distribution of stress tensors for a particular stress stage.

#### 4.3. Results of paleostress tensor determination and paleostress stages

Minor faults with slip lines and joints were measured in 47 different sites, totalling 1075 data. They were inverted to determine the paleostress tensors according to the method described above. The stress inversion results and their correlation allow to define two major paleostress stages: the 'proto rift' and 'active rift' stages (Appendix A). They will be correlated with the classical 'slow rifting' and 'fast rifting' stages defined by Logatchev and Florensov (1978), and discussed in function of the structural and stratigraphic evolution, as summarized above.

The obtained stress tensors are reported on structural maps for each paleostress stage, together with the major faults which were possibly active during this stage (Figs. 7, 9 and 12). The sense of movement along these faults is inferred either from the observed fault kinematics or from the regional stress tensor and the mean fault orientation. The extent of sedimentary basins and volcanic fields displayed corresponds to the situation in the Late Oligocene–Middle Miocene time, compiled from Popova et al.

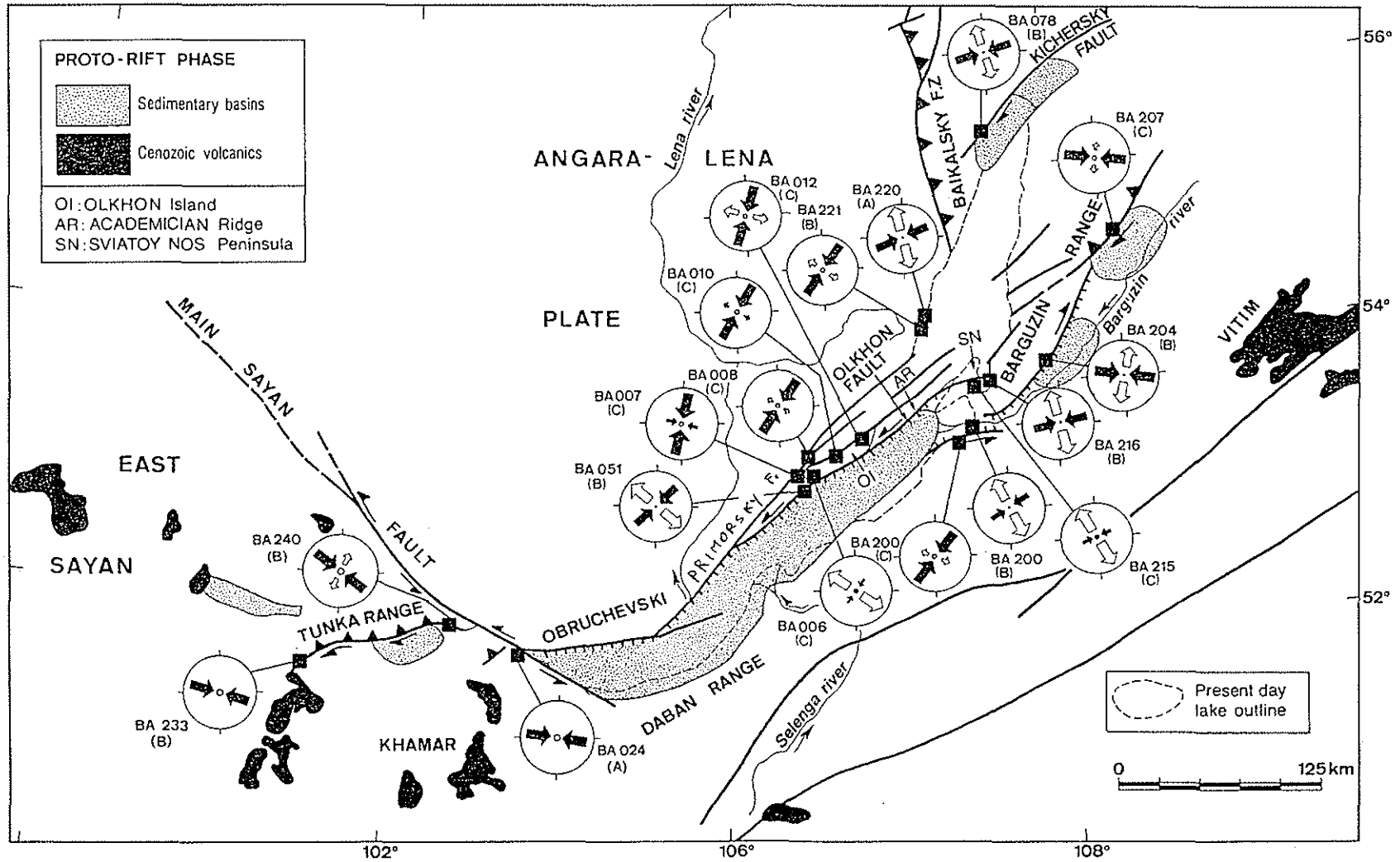


Fig. 7. Structural map with stress symbols for the 'proto rift' phase. Site numbers refer to Appendix A; A-D: quality rank as determined from Table 2. Geology and major structures from Levi et al. (1982). Stress symbols as in Fig. 6.

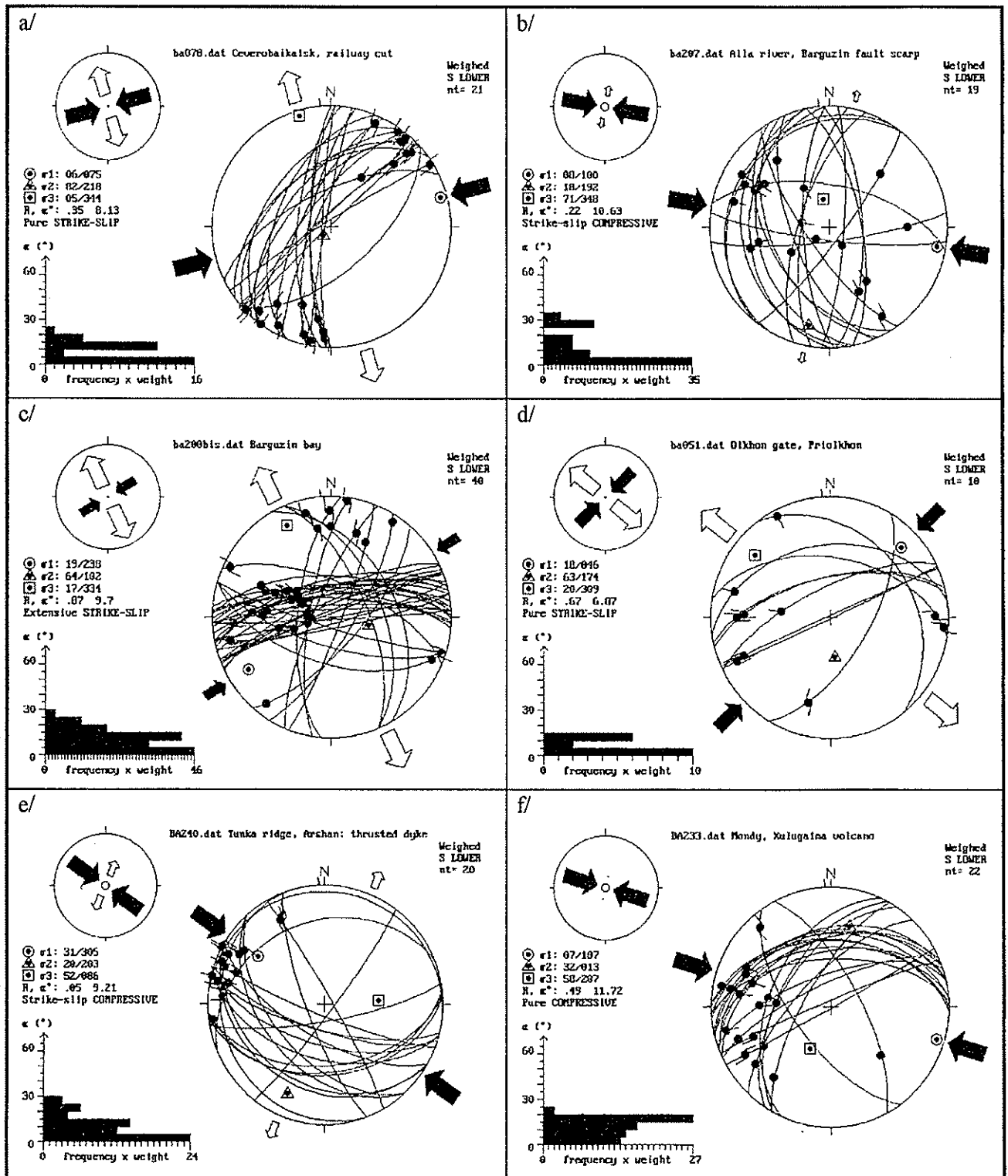


Fig. 8. Examples of stress inversion results for the 'proto rift' phase. Stereograms (Schmidt net, lower hemisphere) with traces of fault planes, observed slip lines and slip senses; histogram of observed slip-theoretical shear deviations  $\alpha$  for each fault plane.

(1989), Logatchev (1993), Rasskazov (1994) and Kazmin et al. (1995).

#### 4.3.1. 'Proto rift' stage

The first Cenozoic paleostress stage represents 18 tensors with 311 fault-slip data (Appendix A1, Fig. 7), recorded in the central part of the rift (North Baikal, Central Baikal and Barguzin basins) and in its southwestern extremity (East Sayan Massif and Tunka depression). All these stress tensors are of the compressional to strike-slip type. They are apparently not related with the present-day stress field, as deduced from earthquake focal mechanisms by Petit et al. (1996).

In the Baikal and Barguzin basins, all measured sites attributed to the 'proto rift' stage are situated in basement rocks, while in the Tunka depression they are found in Miocene basalts.

In the North Baikal and Barguzin basins, the 'proto rift' sites BA078 (Fig. 8a) and BA207 (Fig. 8b) are situated along active normal faults showing multiphase faulting, with strike-slip movement as the oldest and normal movement as the youngest. The remaining sites show only strike-slip faulting, incompatible with the extensional character of the recent Barguzin fault (BA200, Fig. 8c and BA204).

The Olkhon region in Central Baikal is well known for the presence of clay deposits from the Paleogene weathering crust (Kashik and Mazilov, 1994). They are composed of montmorillonite, halloysite, kaolinite and vermiculite, and formed in situ by chemical weathering of the basement crystalline rocks during the Late Cretaceous–Paleogene, under a warm and humid climate (Kotel'nikov et al., 1993). This kind of climate prevailed at least until the Late Oligocene (Popova et al., 1989). These weathering products were not covered by younger rocks, and affected neither by catagenetic nor by hydrothermal alteration (Kotel'nikov et al., 1993). They are generally present as isolated 'pockets' along old fault zones, forming the roots of the paleo-weathering crust.

In the Olkhon region, the measurement sites attributed to the 'proto rift' stage (e.g., BA051, Fig. 8d) typically present the following characteristics: (1) they are located along faults that are presently inactive and do not have clear morphostructural expressions; (2) they affect the products of the Paleogene

weathering crust; (3) they often contain red-orange clay gouge with slickensides; (4) they present a general strike-slip fault kinematics and stress regime, not compatible with the Late Neogene–Quaternary ones (see hereafter); and (5) they often reactivate older, pre-weathering reverse to strike-slip faults (studied in Delvaux et al., 1995). These sites are consequently attributed to the Late Paleogene–Early Neogene period.

In contrast with the Baikal and Barguzin regions, the timing of fault movement for the 'proto rift' stage in the Sayan–Tunka region is better constrained stratigraphically. In the Tunka Range, a steeply dipping, NNE-striking dyke of Miocene basalt described by Ruzhich et al. (1972) is displaced 8 m by a low-angle fault with well expressed slickensides (site BA240, Fig. 8e). This deformation occurred in the post-Middle Miocene, since K–Ar dating of three samples from this dyke gives 9.95, 11.4 and 14.4 Ma (Ruzhich et al., 1972). A transpressional type of stress tensor is reconstructed, with a NW-trending  $S_{Hmax}$  direction. In the western part of the Tunka depression, the Khulugaima volcano, dated at  $16.5 \pm 0.8$  Ma (K–Ar, Bagdasaryan et al., 1981) is also affected by reverse-dextral faults, dipping 35–50° to the NNW (site BA233, Fig. 8f). The stress tensor is pure compressional, with a WNW-trending  $S_{Hmax}$ .

In the Tunka depression, such compressive stress tensors with NW- to WNW-trending  $S_{Hmax}$  were obtained only for sites in Late Miocene volcanics. Significantly different stress tensors were obtained in Late Pliocene–Middle Pleistocene conglomerates (BA222; BA243), in Late Pleistocene sand (BA236) and glacial moraine (BA230). This suggests that in the Sayan–Tunka area, the time range for this compressive deformation and stress field is Late Miocene–Early Pliocene. In addition to these time-constrained sites, site BA024 is situated along the Main Sayan fault, in old (Precambrian?) mylonites, affected by intense polyphase brittle faulting. The three sites (BA240, BA223 and BA024) give a mean tensor of the compressional type, with a WNW-trending  $S_{Hmax}$ .

#### 4.3.2. 'Active rift' stage

The second Cenozoic paleostress stage corresponds to a pure extensional regime in the area

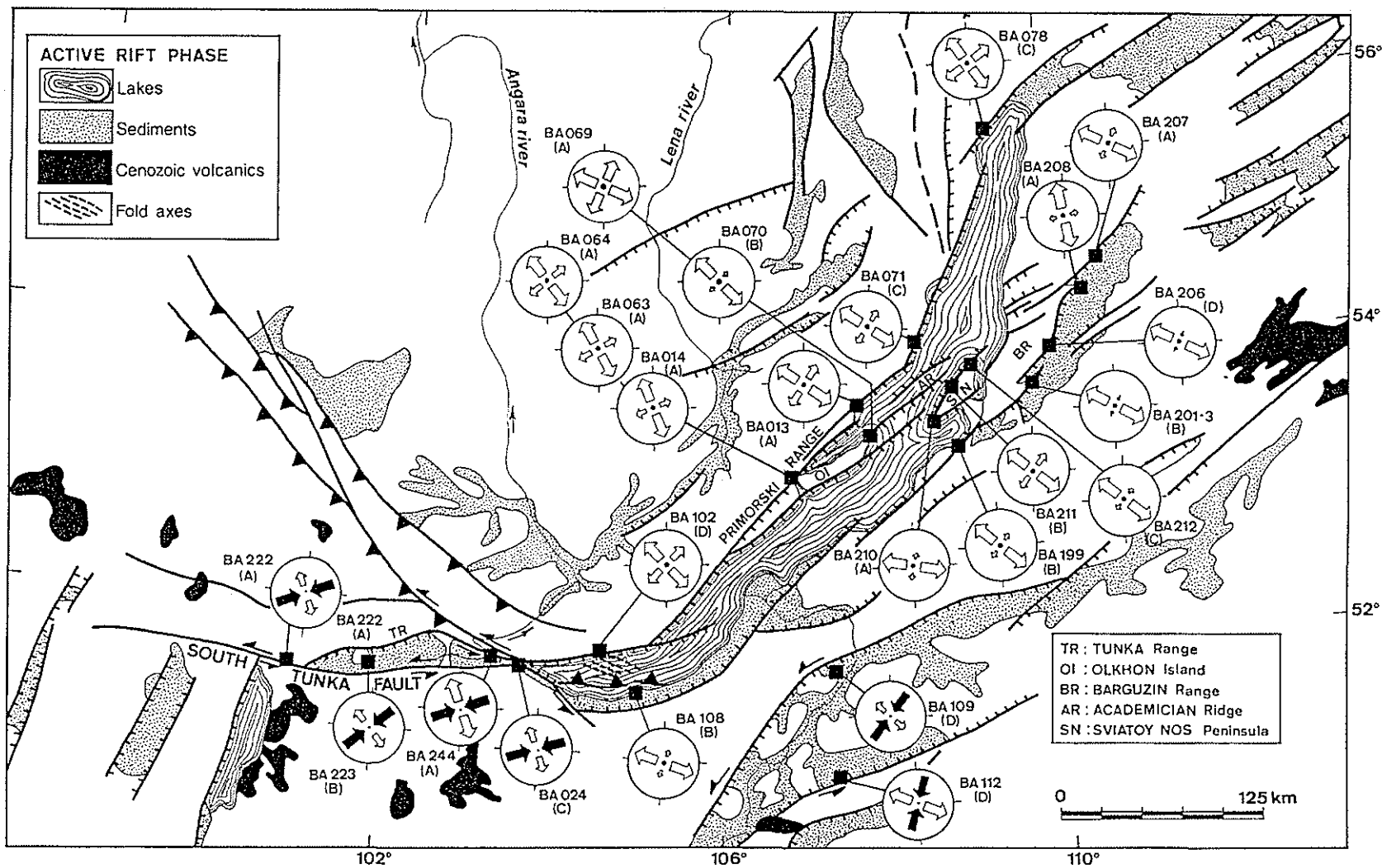


Fig. 9. Structural map for the 'active rift' phase. Site numbers refer to Appendix A; geology and major structures after Levi et al. (1982). Stress symbols as in Fig. 6.

of the Baikal basin itself, and to a strike-slip regime in the Transbaikal and Sayan–Tunka regions (Appendix A2; Fig. 9). Most observation sites are located along fault scarps that have fresh morphological expressions and which control the present-day basin architecture. Along the northwestern coast of the Central and North Baikal basin, several paleoseismic dislocations cutting debris cones and alluvial cones suggest Late Pleistocene to Holocene faulting along the Primorsky and Baikalsky faults (Ufimtsev, 1991). In polyphase sites, the stress tensors referred to the ‘active rift’ stage are always inverted from the youngest set of slickensides.

In the Barguzin graben (e.g., BA207, Fig. 10a) and Sviatoy Nos Peninsula (e.g., BA210, Fig. 10b), stress tensors are mostly of a pure extensional type. Site BA211 was measured in Late Miocene–Early Pliocene sands of the deltaic Sviatoy Nos formation (palynological dating by Kazmin et al., 1995). Along the southern Baikal coast, conjugated joints were measured in the Miocene Thankoy sands (site 108), and the stress inversion gives a WNW–ESE extension, with still an extensional regime (B rank).

In Central Baikal, the best measurement sites for the ‘active rift’ stage were found at the Sarma river mouth, along the Primorsky fault scarp. The fresh and well-preserved morphology of the fault scarp suggests young fault activity. The fault plane itself can be observed at the foot of the scarp, along both banks of the Sarma River (sites BA014 and BA063). Numerous secondary slip planes were found in the upper part of the scarp (site BA064, Fig. 10c). These three sites, totalling 143 fault measurements, give similar tensors after paleostress inversion. These are all of an extensional type, with a slight radial component, implying that  $\sigma_2$  is also extensional. The principal extension ( $\sigma_3$ ) is horizontal and directed almost perpendicularly to the trend of the Primorsky fault. The fault populations are homogeneous (mean deviation angles of 8.5°) and well distributed, with dominant movement planes parallel to the Primorsky fault and well represented conjugate planes. Because of their high quality (A rank), these sites can be selected as reference for the Central Baikal area.

Extensional tensors were reconstructed for other sites along the Primorsky fault (sites BA102, BA013), at the northern extremity of Olkhon Island (sites BA069, BA070), and along the northwestern

coast (site BA071). These tensors are of a similar type as the ones obtained along the Sarma River, but they are constrained by a more limited number of fault data (ranks A to C). In general, the principal extension axis ( $\sigma_3$ ) tends to be perpendicular to the major border fault trace. Along the Kichersky fault in North Baikal, a single site (BA078) shows near-radial extension, but this result is not constrained by enough fault data and, hence, of poor quality (rank C).

In the Transbaikal area, two sites (BA109, BA112) correspond to Cenozoic strike-slip reactivation of Mesozoic faults, but they are of poor quality (rank D). They are also characterized by clay gouge with slickensides. Site BA112 (Fig. 10d) is located along a young morphological tectonic scarp, bordering the Tugnui Mesozoic depression (see Delvaux et al., 1995 for the location of the latter).

In the Tunka depression (Fig. 4 for shaded relief map and Fig. 11 for detailed structure and location), five stress tensors are reported to the Late Pliocene–Middle Pleistocene period. Three of them are stratigraphically well constrained and the others are measured in basement rocks. They are all of the transpressional type, with a consistent ENE-trending  $S_{Hmax}$ . Three sites are situated along the Kultuk River, in the vicinity of the South Tunka fault. At the eastern side of the Tunka depression, site BA244 in the Bistraya sub-basin is measured in tilted (40–70°SSE) conglomerates of the same type and age as the one in Mondy, and covered unconformably by undisturbed Late Pleistocene terrace of the Kultuk River (Fig. 10e). The WNW trend of the tilted beds (N305°E) corresponds closely to the direction of the intermediate  $\sigma_2$  axis of the stress tensor obtained from the measurement of faults and joints which affect them (N339°E). This suggests that both the folding and the faulting correspond to the same deformation, the folding being slightly older than the faulting. In the Mondy sub-basin, at the western extremity of the depression (site BA222), a thick layer (>40 m) of conglomerate of probably Early–Middle Pliocene age is affected by a series of subvertical E–W-striking right-lateral faults, for which a strike-slip type of tensor was reconstructed (Fig. 10f). In the central part of the Tunka depression, Late Miocene basaltic deposits along the South Tunka fault, against the Nilovsky Spur are also affected

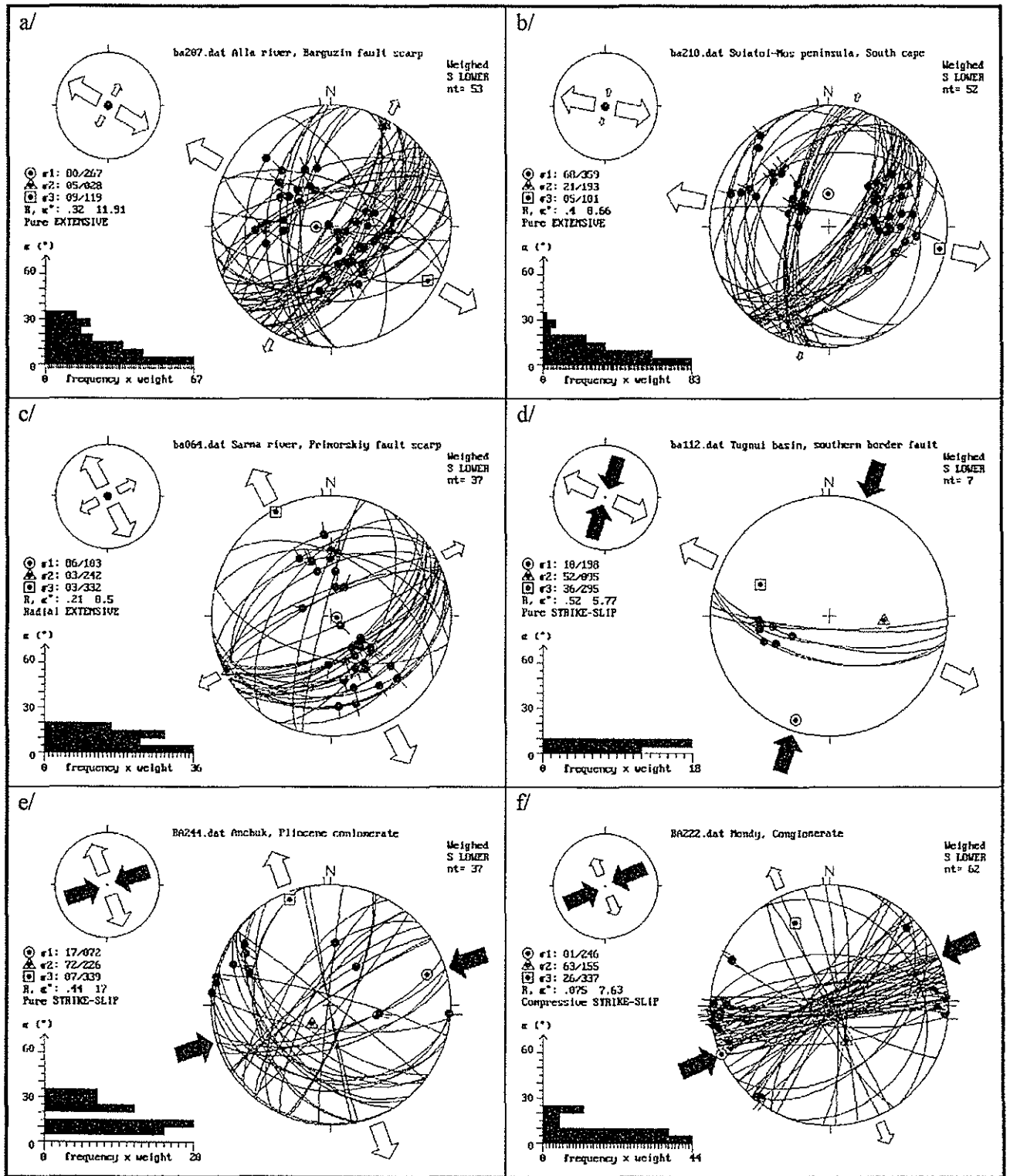


Fig. 10. Examples of stress inversion results for the 'active rift' phase (Late Miocene–Middle Pleistocene in the Tunka area). Stereonets as in Fig. 8.

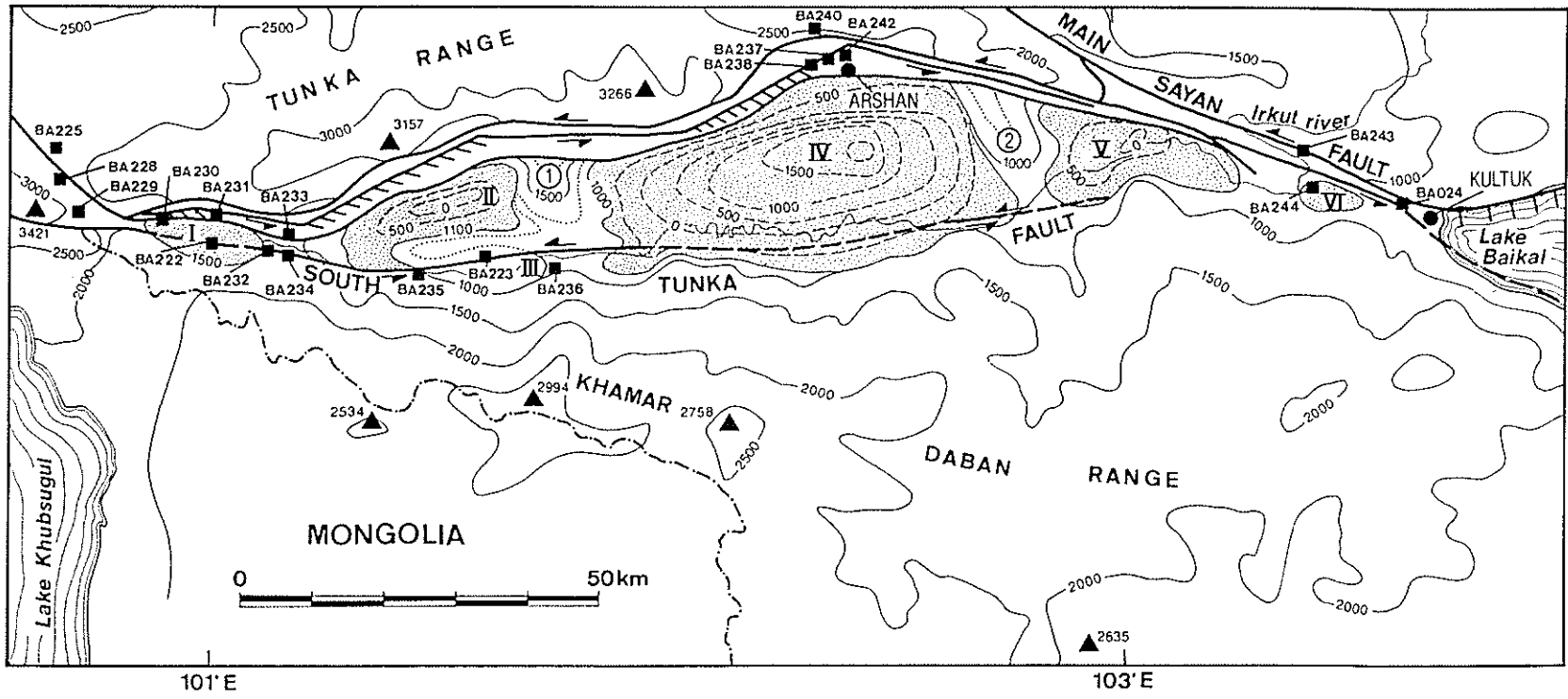


Fig. 11. Structure and basement topography of the Tunka area, redrawn from Sherman and Ruzhich (1973). Depth of basement is inferred from geophysical exploration and drilling. Fault kinematics is estimated from major fault orientation and mean stress regime for the 'active' rift stage (Late Pliocene–middle Pleistocene substage). Isolated sedimentary sub basins: I = Mondy; II = Khoitogol; III = Turan; IV = Tunka; V = Tori; VI: Bistraya. Intrabasinal basement highs: 1 = Nilovsky Spur; 2 = Elovsky Spur.

by E–W-striking dextral-strike-slip minor faults with clay gouge (site BA223). This site recorded two different stress states, with a transpressional regime as the oldest one and a normal faulting regime as the youngest. The transpressional regime has an ENE–WSW  $S_{Hmax}$  direction and correlates well with sites BA244 (Bistraya) and BA222 (Mondy). The tensor of site BA024 was obtained from a polyphase site along the Main Sayan fault.

The last five tensors of the Tunka and South Baikal regions are stratigraphically constrained to the Late Pleistocene–Holocene period (Fig. 12). In the Selenga delta, site BA125 is measured in Holocene sands along the scarp created by the 1862 historical earthquake that caused the disappearance of a great part of the delta under the water, together with several villages. An extensional-type of tensor is inverted from systems of conjugated joints (Fig. 13a). In Arshan, at the foot of the Tunka Range, a series of joints, some of which conjugated, were measured along a Holocene tectonic scarp (site BA242: Fig. 13b). Measurements were also made in the sand quarry described by McCalpin and Khromovskikh (1995). Further west, conjugated joints and fractures with apparent normal displacement were measured in Late Pleistocene sands along the South Tunka fault (site 236 Turan: Fig. 13c). They show a combination of pure strike-slip movements along subvertical E–W planes, parallel to the general trend of the South Tunka fault, and oblique–normal movements along NW-dipping, NE-striking faults. In site BA223, against the Nilovsky Spur, the second set of faults with slickensides that affect the Late Miocene basalts give a tensor compatible with the Late Pleistocene–Holocene regime. Finally, recent faulting is observed at the margin of the Mondy sub-basin, displacing Late Pleistocene moraine deposits overlying basement rocks (Site BA230: Fig. 13d). Close to this site, the moraine deposits are affected by seismic dislocations related to the Mondy  $M$  6.6 earthquake of April 4, 1950.

As a stratigraphic control, the ‘active rift’ stage appears to begin in Late Pliocene and thus corresponds to the ‘fast rifting’ stage of Logatchev (1993). In the Tunka depression, a better age constraint allows to divide the ‘active rift’ stage in a Late Pliocene–middle Pleistocene and a Late Pleistocene–Holocene substage.

#### 4.4. Evolution of the regional stress field with time

##### 4.4.1. ‘Proto rift’ stress field

The ‘proto rift’ stress field has three major characteristics: (1) the direction of horizontal principal stress axes ( $S_{Hmax}$ ) displays a curved trajectory; (2) the average stress regime is dominantly compressional in Sayan–Tunka and transpressional in Central Baikal–Barguzin; and (3) there is a wide variety of stress regimes in the Baikal–Barguzin area, with individual regimes ranging from transpressional to transtensional.

The  $S_{Hmax}$  direction trends NE in Central Baikal, parallel with the margin of the Angara–Lena Platform, and E–W in both extremities (East Sayan, North Baikal and Barguzin). This pattern is difficult to explain, as data from the neighbouring regions for this period are lacking.

A clear change of stress regime along the rift trend is indicated by the ‘proto rift’ paleostress data, as show by the index  $R'$ . The average stress regime is dominantly compressional in the Sayan–Tunka area ( $R' = 2.37$ ), transpressional in Central Baikal ( $R' = 1.70$ ), Barguzin Range ( $R' = 1.96$ ) and Northwest Baikal ( $R' = 1.65$ ), and transtensional in the Sviatoy Nos area ( $R' = 1.27$ ). This suggests lateral variations of relative stress magnitudes, with stress concentration in the Sayan–Tunka area and stress relaxation in the Sviatoy Nos area.

In Central Baikal and Barguzin, the stress tensors of the ‘proto rift’ phase exhibit a general strike-slip stress regime, with large fluctuations from transpression to transtension. The individual stress regimes, expressed by the index  $R'$ , are displayed in Fig. 14a. It appears that the ‘proto rift’ stress tensors display a large distribution of stress regimes, from pure compressional ( $R' = 2.69$ : site BA007) to transtensional ( $R' = 0.87$ : site BA215). This pattern can be interpreted in two different ways: (1) it may correspond to a mean regional strike-slip stress regime with  $R' = 1.53$  (weighed as a function of the number of faults), with local transpression and transtension, or (2) it may represent a general evolution of the stress regime with time, from transpression to transtension. One site, with two different paleostress tensors attributed to the ‘proto rift’ stage (BA200), shows that the transpressional regime may be older than the transtensional one.

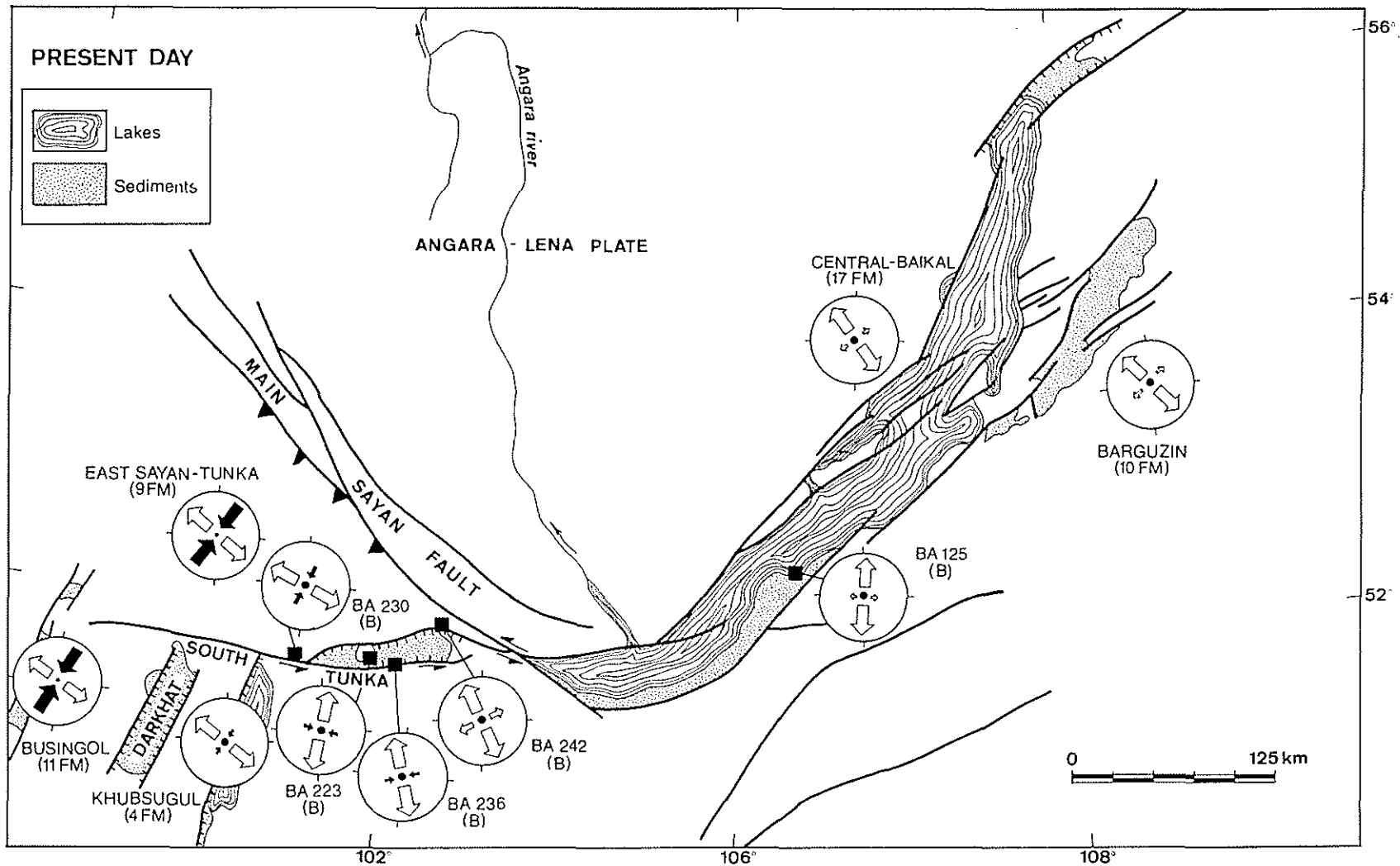


Fig. 12. Structural map for the Late Pleistocene–Holocene in the Tunka and South Baikal basins. Site numbers refer to Appendix A; geology and major structures after Levi et al. (1982). Stress symbols as in Fig. 6.

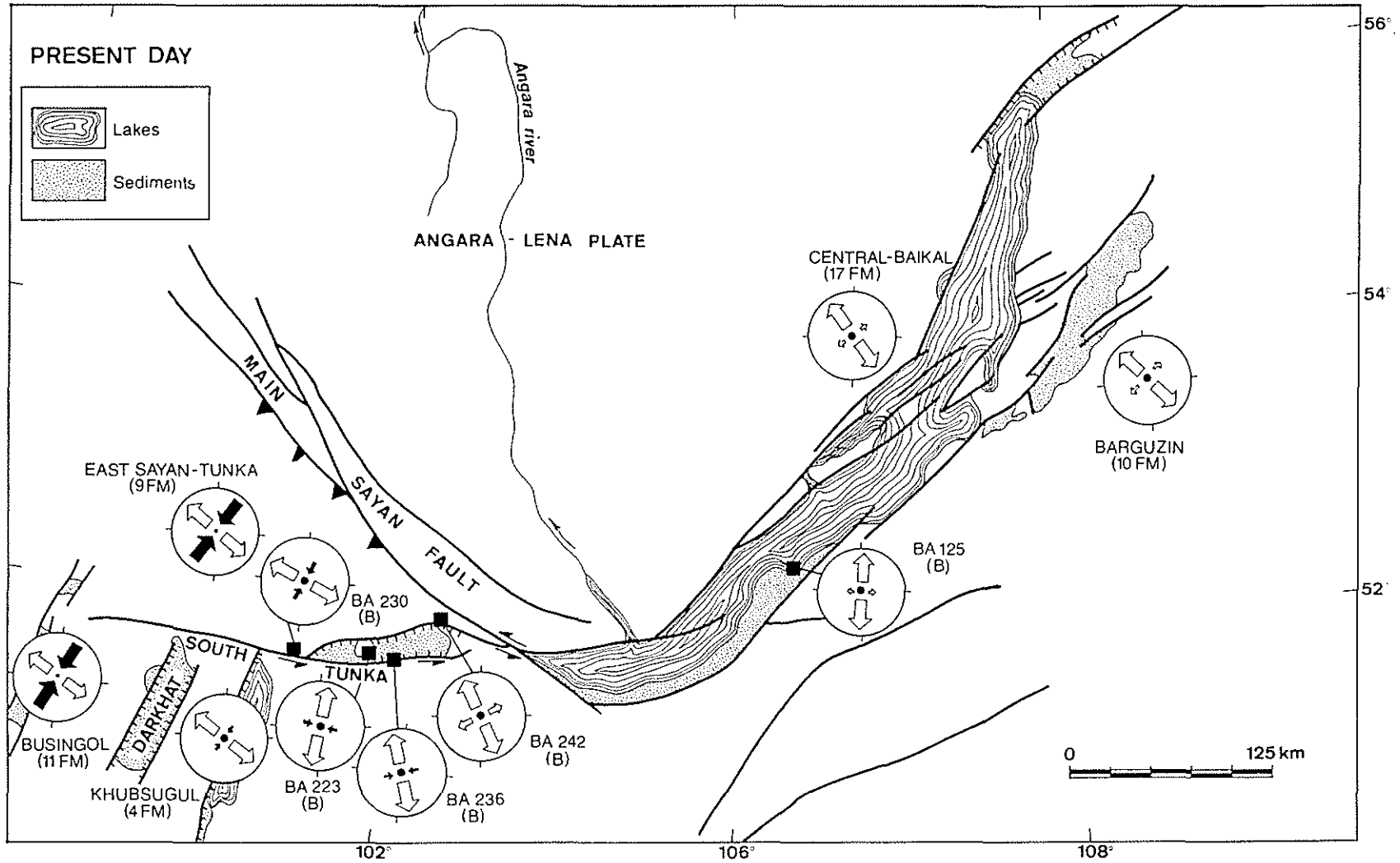


Fig. 12. Structural map for the Late Pleistocene–Holocene in the Tunka and South Baikal basins. Site numbers refer to Appendix A; geology and major structures after Levi et al. (1982). Stress symbols as in Fig. 6.

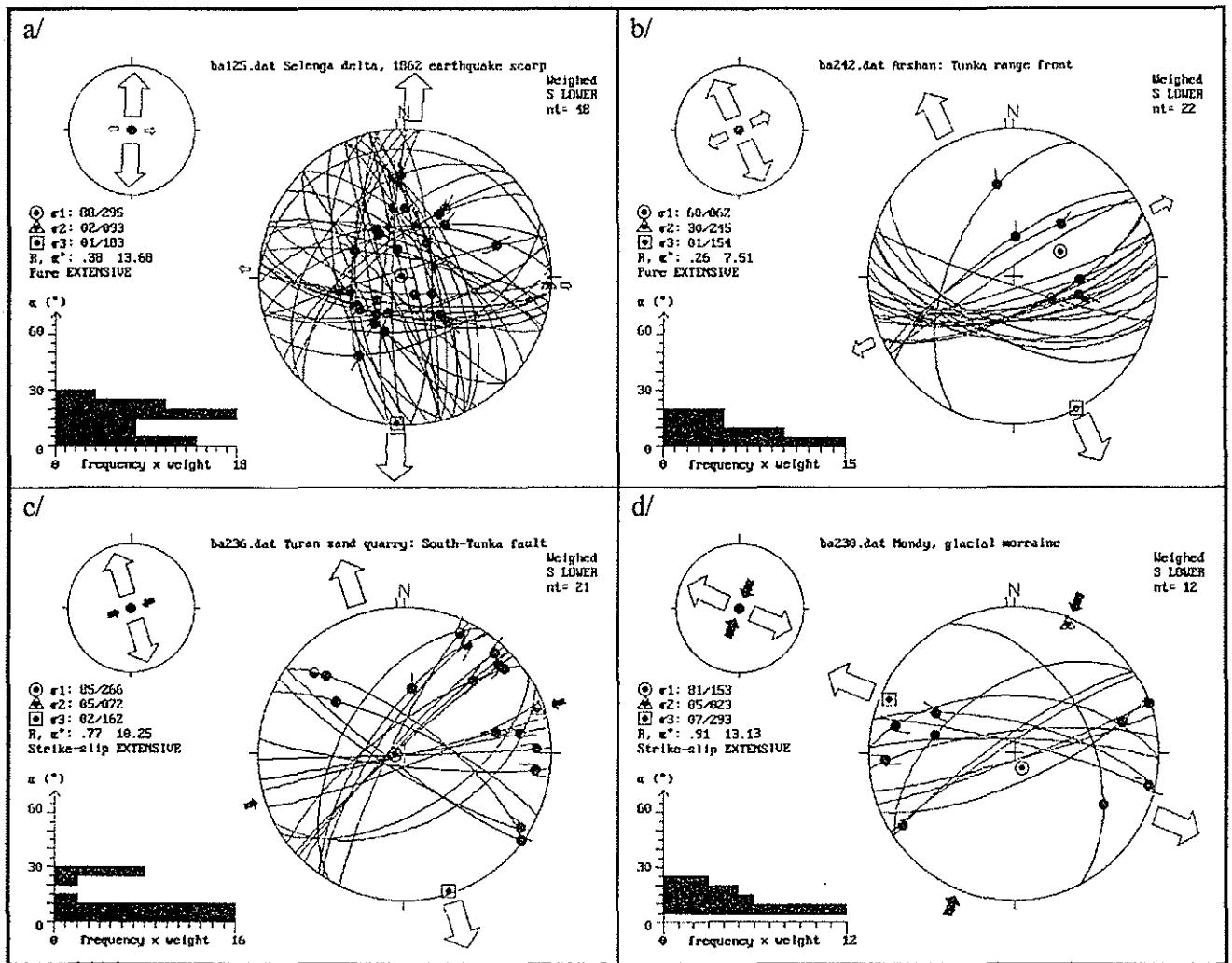


Fig. 13. Examples of stress inversion results for the 'active rift' phase (Late Pleistocene–Holocene). Stereograms as in Fig. 8.

In conclusion, direct and indirect evidences allow to consider the 'proto rift' paleostress field, as time-equivalent to the 'slow rifting' stage defined by Logatchev and Florensov (1978). The age of the latter is estimated on the basis of the stratigraphic and structural evolution of the Baikal Rift as Late Oligocene–Early Pliocene (Logatchev, 1993; Rasskazov, 1994). This stage ended by a marked change in tectonic regime and stress field, that characterizes the onset of the 'active rift' stage.

4.4.2. 'Active rift' stress field

The good regional distribution of the sites in the studied region allows to assess the 'active rift' stress field. In general, the mean direction of hor-

izontal principal stress ( $S_{Hmax}$ ) is relatively constant (North Baikal N055°E, Barguzin N041°E, Central Baikal N041°E, Ulan-Ude N027°E and Tunka N034°E), while the stress regime changes regionally. Pure extension characterizes the Barguzin rift ( $R' = 0.45$ ) and most part of the Central Baikal region ( $R' = 0.38$ ). Southwards and westwards, the stress regime evolves into pure strike-slip, both in the Transbaikal region ( $R' = 1.81$ ) and in the Tunka depression ( $R' = 1.70$ ). The transition between the two regimes occurs somewhere in the South Baikal basin, but our data set does not allow to locate it precisely.

In the Tunka region, it is possible to show an evolution of the stress field during the 'active rift'

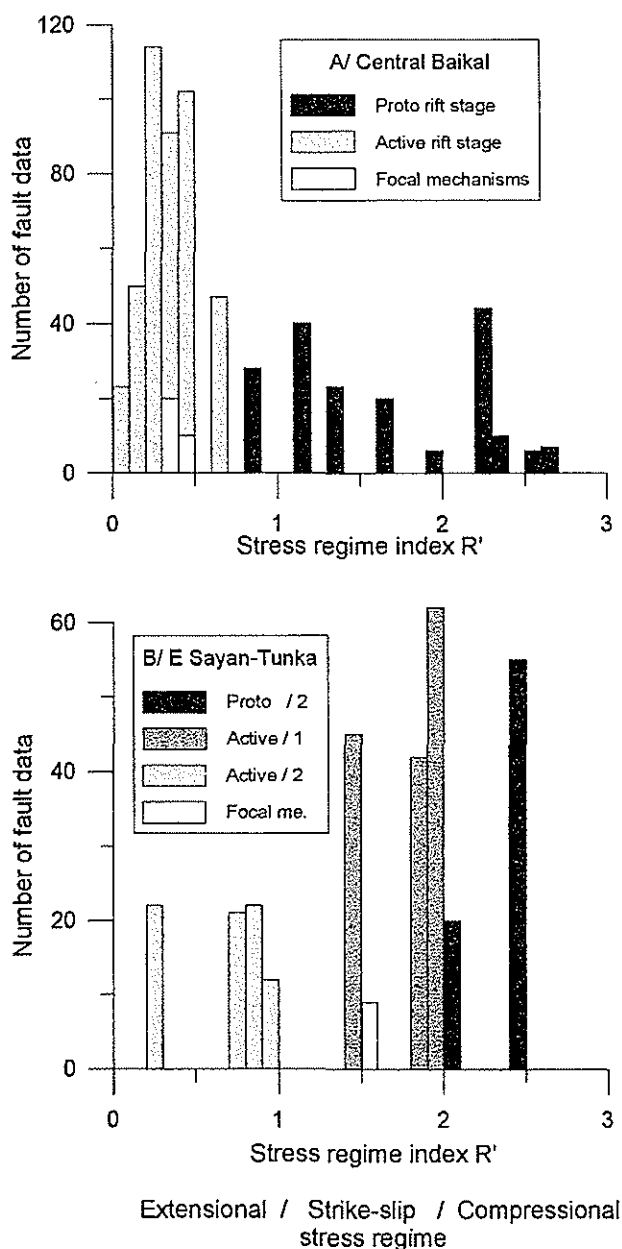


Fig. 14. Bar diagram showing the stress regime index  $R'$  in function of the number of data used in stress inversion. (a) Central Baikal area (North and Central Baikal basins, Barguzin basin). (b) East Sayan-Tunka area.

stage itself. The mean stress regime was more extensional during the Late Pleistocene-Holocene period ( $R' = 0.65$ ) than it was during the Late Pliocene-Middle Pleistocene period ( $R' = 1.81$ ). However, the inversion of nineteen focal mechanisms for the whole East Sayan block gives a pure strike-slip stress tensor ( $R' = 1.58$ ), with a NE-SW-trending  $S_{Hmax}$

direction, at a right angle to the Main Sayan fault (Petit et al., 1996).

In the stress regime diagram (Fig. 14a), the stress tensors of the 'active rift' phase for Central Baikal are well grouped in the extensional field. The index  $R'$  of individual sites is generally comprised between 0.2 and 0.5, indicating a pure extensional regime, with a radial component. No overlap exists with the field corresponding to the stress tensors of the 'proto rift' phase. This suggests that the two stress regimes are significantly different and that a clear break existed in the stress field evolution from the 'proto rift' to the 'active rift' stage in Central Baikal. In the East Sayan-Tunka area, the stress field evolves continuously with time towards a more extensional regime (Fig. 14b). The break between the two rift stages is marked by a slight shift of the stress regime to the strike-slip field, and by a 45° anticlockwise rotation of the horizontal stress axes. During the 'active rift' stage itself, the stress field evolves rapidly towards an extensional regime in the central part of the Tunka depression. However, the latter seems to be relatively unstable since the focal mechanisms for the East Sayan-Tunka area indicate that the regional present-day stress regime is pure strike-slip.

From the above, we conclude that the stress field in the Baikal Rift System changed markedly in the Late Pliocene. It became pure extensional in the North and Central Baikal areas and strike-slip in the East Sayan and Tunka areas. The South Baikal basin lies in a transitional position between these two stress provinces. This stage is defined as the 'active rift' stress field and is time-equivalent to the 'fast rifting' stage of Logatchev and Florensov (1978).

#### 4.4.3. Present-day stress field

At the scale of Central Asia, the present-day stress field evolves from a compressional regime in the Tian Shan and SW Altai, to strike-slip regime in the Sayan block, and to pure extension in the Baikal Rift System (Tapponnier and Molnar, 1979; Solonenko, 1993; Petit et al., 1996; Solonenko et al., 1997). At the northwestern extremity of the Baikal Rift System, the stress field changes back to a strike-slip regime, in the Olëkma-Stanovoy belt (Parfënoy et al., 1987). For the whole area, the horizontal principal compression trends generally NE (except for Lake Zaisan), with only changes in the rela-

tive principal stress magnitudes. This suggests that the influence of far-field compressional stress which characterizes most of Central Asia is still perceptible in the Baikal Rift System. As noted by Petit et al. (1996) the transition from the extensional stress field of the rift zone to the plate-scale compressional stress field of Central Asia is progressive at the southern extremity of the rift zone, and rather sharp at its northeastern extremity.

For the region covered by our field investigation, the mean stress tensors of the 'active rift' stage for the different segments of the rift are remarkably similar to the stress tensors inverted from earthquake focal mechanisms by Petit et al. (1996), both in stress regimes and stress axes orientation. This implies that the stress regime of the 'active rift' stage is similar to the present-day stress regime.

Summarising the above results, it appears (1) that the stress field of the 'active rift' stage which started in the Late Pliocene is still acting today, and (2) the rift-type extensional stress field of the Baikal Rift System is limited laterally on both rift extremities, by regions affected by plate-scale compressive to strike-slip stress fields.

## 5. Fault kinematics and basin evolution

After defining the stress field evolution in time and space, the next step in our investigation is to reconstruct the fault kinematics and relative movement of major tectonic blocks. The fault data sets used for stress tensor inversion can also be used for computing the mean movement planes and slip line directions along major faults. The principal movement planes of all sites are obtained by separating the total data set into homogeneous subsets and computing the mean orientation of each subset by the technique of Huang and Charlesworth (1989). The slip vector on these planes is reconstructed by applying the corresponding stress tensor with the method of Means (1989).

The local and regional movement planes, with their slip directions and senses are given in Appendix B. The regional slip vectors are used as a rough estimation of the relative movement between adjacent blocks (Table 2 and Fig. 15).

### 5.1. Rift initiation in a transpressional to transtensional context ('proto rift' stage)

The 'proto rift' kinematics of the Central Baikal basin is well documented in the Olkhon region. The Olkhon fault, bordering the southeastern flank of Olkhon Island and the underwater Academician Ridge, appears to be a steeply SE-dipping sinistral strike-slip fault with a normal component. It controlled the subsidence of the Central Baikal basin, developing as a half-graben until the Middle Miocene (Kazmin et al., 1995). The change of stress regime from transpressional to transtensional in Central Baikal may be correlated with the onset of extensional faulting observed by Kazmin et al. (1995) in the seismic profiles of the Academician Ridge area. It marks the beginning of the land barrier disruption between the North and Central Baikal basins, in the Late Miocene–Early Pliocene.

In the Barguzin depression, sedimentation also occurred in the Miocene (Popova et al., 1989), but the poor stratigraphic knowledge of these deposits did not allow to determine when it started. Sedimentation was probably controlled by the activity of the fault system in front of the Barguzin Range. The movement inferred from fault kinematics suggests that it was a dextral strike-slip fault with a normal component in the southern sub-basin and a reverse component in the northern sub-basin. This dextral movement is opposite to the sinistral movement which occurred along the Olkhon fault, of a similar ENE trend. The difference is apparently due to a change in the  $S_{Hmax}$  direction, from a NE trend in the Olkhon region to an E–W trend in the Barguzin region.

In Oligocene–Middle Miocene time, no significant sedimentation occurred in the North Baikal basin (Hutchinson et al., 1992), except in its northernmost part, at the foot of the Kichersky fault (Popova et al., 1989). Further to the northwest, reverse movement is inferred along the N–S-striking Baikalsky fault, at the contact with the Angara–Lena Platform (from interpretation of the Neotectonic map of Levi et al., 1982).

The Tunka depression developed between the Tunka Range front and the South Tunka fault (Fig. 11). It presently consists of a series of five isolated depressions separated along trend by basement

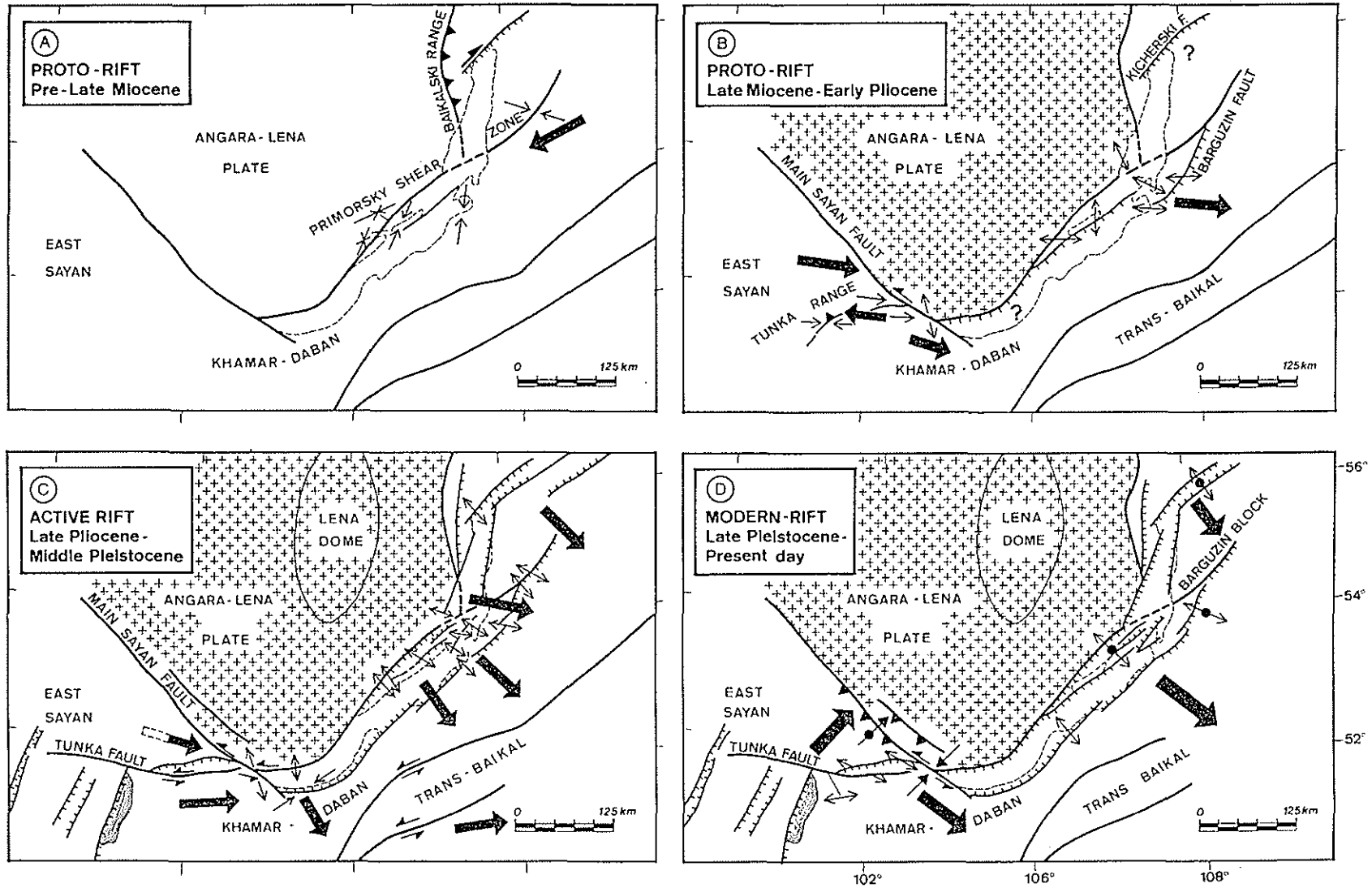


Fig. 15. Map of predicted slip vectors and tectonic interpretation for the four kinematic sub-stages. Data from Appendix B. Divergent and convergent arrows correspond to normal and reverse faults, respectively. Arrow pairs of opposite sense correspond to strike-slip faults. Data from earthquake focal mechanisms are indicated with a dot on the arrow. Large arrows represent inferred block motion relative to the adjacent block or with respect to the Angara-Lena Platform.

Table 2

Inferred azimuthal directions of block movements relative to the 'stable' Angara–Lena Platform, based on the mean slip vectors calculated from fault slip data and from earthquake focal mechanisms of Petit et al. (1996)

Major rift stages Inferred movement directions/substages	Proto rift phase		Active rift phase	
	(a) pre-Late Miocene	(b) Late Miocene– Early Pliocene	(c) Late Pliocene– Early Pleistocene	(d) Middle Pleistocene– Holocene
Opening Kichersky + North Barguzin basins	222		138	149
Opening south extremity North Baikal basin			108	
Opening north extremity South Baikal basin	244	101	134	133
Opening Small Sea/Olkhon block			130	
Opening South Baikal basin Khamar Daban relative to Angara–Lena Platform		116	151	?
Transbaikal region relative to Khamar Daban		X	052	?
Khamar Daban relative to East Sayan		273	084	125
East Sayan relative to Angara–Lena Platform		096	105	042

highs (Sherman and Ruzhich, 1973). The geometrical setting and facies distribution of the Miocene sediments and volcanics demonstrate that the Tunka depression had a very different form in the Miocene than at present (Kashik and Mazilov, 1994). It can be inferred that the original depression developed as a single basin, at the foot of the Tunka Range. In cross-section, the Tunka depression corresponds to a relatively symmetrical flexure, as opposed to the half-graben profile of the Olkhon block in Central Baikal (Fig. 16). The age-constrained fault kinematics of outcrops BA233 and BA240 indicates that the Tunka Range was an oblique-thrust front in the Late Miocene–Early Pliocene. All this suggests that the Tunka depression initially developed as a flexural basin, at the foot of a thrust range front.

At the SW margin of the Angara–Lena Platform, sinistral strike-slip movement may have occurred along the Main Sayan fault, in association with oblique thrusting in the Tunka Range itself. In this situation, a lateral southeastwards escape of the East Sayan Massif relative to the stable Angara–Lena Platform is expected to have taken place along the Main Sayan fault, at least in the Late Miocene–Early Pliocene period (Fig. 15b). The southeastwards movement of the East Sayan Massif is accommodated by extensional tectonics in the South Baikal basin and compressional tectonics in the East Sayan Massif itself.

The Late Miocene–Early Pliocene transtensional stage in Central Baikal occurs synchronously with the 'proto rift' paleostress regime recorded in East

Sayan–Tunka. For the latter, no paleostress tensors were recorded for the period pre-dating the Late Miocene, despite that the development of the sedimentary basin was already active. As a consequence, for both studied areas it seems that a Late Miocene–Early Pliocene substage can be identified. It forms the second half of the 'proto rift' stage.

To summarise, the 'proto rift' stage has to be subdivided into a pre-Miocene substage and a Late Miocene–Early Pliocene substage. In the pre-Late Miocene (Fig. 15a), rifting was initiated by wrench fault reactivation of the Primorsky shear zone, at the boundary between the Angara–Lena Platform and the Khamar Daban–Barguzin block, under transpressional conditions. In the Late Miocene–Early Pliocene (Fig. 15b), the central part of the rift started to open obliquely. On the other side of the Angara–Lena Platform, the eastwards movement of the East Sayan block by left-lateral translation along the Main Sayan fault resulted in the lateral expulsion of the Khamar Daban block and the oblique opening of the South Baikal basin as a space accommodation process. Decoupling of the Khamar Daban block relative to the East Sayan block along the Tunka fault resulted in oblique thrusting in the Tunka Range and formation of the Tunka basin as a footwall flexure.

### 5.2. Active rifting in extensional context (active rift stage)

The fault kinematics for the 'active rift' stage in the Barguzin and Central Baikal areas is dominantly

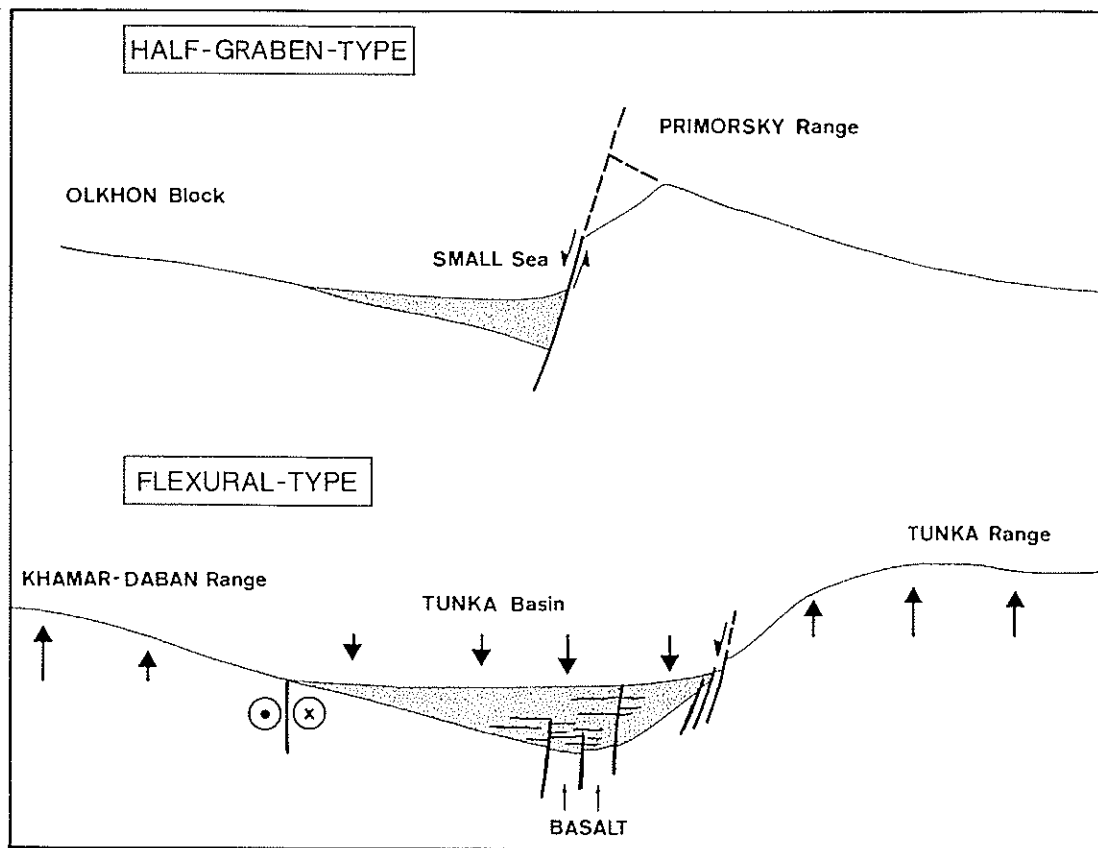


Fig. 16. Flexural-type profile of the Tunka basin, compared with the half graben-type profile of the Olkhon block in Central Baikal. For the Tunka profile: 1:1 vertical/horizontal scales and depth of basement inferred from borehole and geophysical exploration (after Ruzhich et al., 1972).

normal dip-slip faulting along the major NE- to ENE-striking border faults. Our data show that a limited lateral component may occur along some of the master faults, generally with a sinistral slip sense, but not systematically. This can be explained by a slight obliquity of the major fault system relative to the principal stress axes, but it does not support the model of pull-apart opening along E–W sinistral transcurrent faults proposed by Balla et al. (1991).

In the northern extremity of Lake Baikal, the Kitchera basin (Fig. 2) became symmetrical during the ‘active rift’ phase, while the Baikalsky fault was inverted into a normal fault, bordering the Baikalsky Range on its eastern side.

In Transbaikal, recent fault kinematics data are scarce, but morphostructural observations indicate that this region has presently a moderate tectonic activity. Deformation occurs mainly by strike-slip and oblique slip reactivation of the Mesozoic fault system.

In East Sayan, our results highlight the importance of the South Tunka fault which acts as a transform zone to accommodate the opening of the N–S grabens of Busingol, Darkhat and Khubsugul in Mongolia (Fig. 15c, d). The Tunka depression itself is located along the Tunka transform, bordered to the south by the South Tunka fault, but limited to the north by the Tunka fault at the foot of the Tunka Range. The latter has a curved shape, dipping to the south and is interpreted by Sherman and Ruzhich (1973) as an oblique-normal fault with a left-lateral component. Along this fault, microstructural data were obtained only for the Holocene period (BA242). In accordance with Sherman and Ruzhich (1973), we found a significant normal movement, combined with a slight left-lateral component.

The South Tunka fault is rectilinear, with an along-trend alternation of uplifted and subsided blocks, typical for a strike-slip fault (Fig. 4). The fault kinematic data of outcrops BA222, 223 and 244

demonstrate that sinistral movement occurred along the South Tunka fault since the Late Pliocene. The shaded relief map (Fig. 4) illustrates the tectonic nature of the two basement highs which separate the Koitogol, Tunka and Bistraya sub-basins: the Nilovsky and Elovsky spurs (Fig. 11). They appear as asymmetric ramps, SW-tilted and bounded on the northeastern side by NW-striking reverse faults. They pierce all the sediments of the Tunka depression, Middle Pleistocene included. This structure can be best explained as the manifestation of compressional deformation under the recent stress field with NE-trending  $S_{Hmax}$ . Compared with the situation in the Late Miocene–Early Pliocene, a major change in tectonic regime occurred in the Late Pliocene, with development of the South Tunka strike-slip fault and oblique deformation of the Tunka depression itself. This corresponds to a  $\pm 45^\circ$  clockwise rotation of the  $S_{Hmax}$  direction and a change of stress regime from compressional ( $R' = 2.37$ ) to transpressional ( $R' = 1.81$ ).

Deformation of the area adjacent to the Tunka fault near Arshan was surveyed by repeated geodetic measurements of eleven triangulation points in 1975 and 1978 in the Tunka Geodynamic Polygon (Kesselman et al., 1992). This survey shows that the area of dynamic influence of the fault is 3–5 km, and that the Tunka area underwent a general ENE–WSW shortening with an ESE–WNW extension, in agreement with the principal deformation axes inferred from focal mechanisms. In the Talaya geophysical underground station, near Kultuk at the western end of South Baikal, quartz extensometer measurements for the years 1990–1991 show strain axes which are also coaxial with the regional stress axes (Timofeev et al., 1994).

To the southwest the Angara–Lena Platform is separated from the East Sayan uplift by a series of NW-striking faults. The topography is progressively depressed across this fault zone, from more than 3000 m high in the East Sayan Massif to 400 m high in the Angara valley. The Main Sayan fault marks the boundary between the Siberian Craton and the East Sayan block. It has the typical linear morphology of a strike-slip fault (Fig. 4). The Main Sayan fault generally trends NW and is bent progressively to a WNW-trend in the vicinity of the South Baikal basin. It forms a transfer zone between the Tunka and the

South Baikal depressions and terminates abruptly at the southern side of the South Baikal basin. The Angara fault separates the Angara depression from the uplifted margin of the Angara–Lena platform (Sharyzhalgay Archean complex), reactivating a Mesozoic thrust system (described in Delvaux et al., 1995). It forms a clear WNW-striking morphological break on the digital terrain model (Fig. 4). Reverse faulting along this line is suggested by the presence of earthquakes with reverse mechanisms in the East Sayan area. The tectonic movement between the Angara–Lena Platform and the East Sayan Massif is partitioned between these two faults, which also forms a large-scale asymmetric positive flower structure.

The dominant  $S_{Hmax}$  direction for this area is  $N061^\circ E$  (Late Pliocene–middle Pleistocene fault data) to  $N034^\circ E$  (focal mechanism data). The stress regime is strike-slip ( $R' = 1.81$  to  $1.52$ ). An oblique-reverse movement is inferred along the NW-trending segment of the Main Sayan fault, and a sinistral strike-slip movement along the NNW-trending segment. Morphological evidence also argues for recent sinistral movements along this fault, between the Tunka Range and the South Baikal basin. Near Kultuk, a small thalweg is sinistrally offset by 5 m along a paleoseismic dislocation parallel to the major fault. On a larger scale, both the Irkut and Arkhut rivers that cross the Main Sayan fault are offset sinistrally by  $15 \text{ km} \pm 500 \text{ m}$  (offset valleys indicated by black arrows in Fig. 4). Supposing that this displacement is related to the last tectonic stage, from the Late Pliocene to the Present (3 Ma), the mean lateral slip rate is  $5 \pm 0.2 \text{ mm/yr}$ . It is the maximum possible rate, because the bending of the two rivers might have been influenced by earlier fault movements.

Late Cenozoic deformation also affected the central part of the Angara–Lena Platform. The Lena Dome forms a large-scale domal uplift, rising more than 1000 m above the Angara and Kirenga depressions (Figs. 2 and 3). Both the Lena Dome and the Primorsky rift shoulder uplift formed recently. This is shown by the presence of the former Buguldeika–Manzurka–Lena river, flowing out of Lake Baikal across the Primorsky Range until the Early Pleistocene, and deeply incised into the Lena Dome (Mats, 1993). The combined uplift of the Lena Dome and the Primorsky–Baikalsky rift shoulder led

to the development of a rim of shallow basins at the margin of the Angara–Lena Platform.

In summary, orthogonal opening characterizes the whole duration of the ‘active rift’ stage in the Central Baikal, North Baikal and Barguzin basins (Fig. 15c, d). Oblique opening of the South Baikal basin is still operating as a space accommodation process due to the left-lateral expulsion of the Khamar Daban Massif relative to the Angara–Lena Platform. This lateral movement is transmitted to the Transbaikal area where the Mesozoic structures are reactivated. It is different from the previous, Late Miocene–Early Pliocene, stage in that the relative movement between the Khamar Daban range and the East Sayan block changed from oblique thrusting to a left-lateral translation. This results in the appearance of the South Tunka strike-slip fault which controls the formation of the modern Tunka depression and accommodates the opening of the Khubsugul, Darkhat and Busingol depressions. The former unique flexural depression of Tunka is now reformed by the formation of secondary ramps oblique to the master faults. The tectonic setting of the Tunka depression evolved from pure strike-slip in the Late Pliocene–middle Pleistocene to transtensional in the Late Pleistocene–Holocene. In the meanwhile, movement of the East Sayan block relative to the Angara–Lena Platform is dominated by oblique sinistral-reverse faulting along the Main Sayan fault. Deformation also propagated to the Angara–Lena Platform, by the reactivation of an older Mesozoic marginal thrust system, and by the development of the Lena Dome in its central part.

## 6. Conclusion

The results of paleostress and present stress analysis show that the Cenozoic stress field in the Baikal Rift System evolved both in time and space. The different stages of basin evolution and rifting are related to changes in the paleostress field. The present stress field is in continuity with the stress pattern of Central Asia. Extensional stresses prevail in most of the Baikal Rift System in the middle of the Eurasian plate which is affected mainly by a strike-slip to compressional stress field. Throughout the Cenozoic, the stress regime was different on both sides of the southern margin of the Angara–Lena

platform. During each stage of rift evolution, the stress field was more compressional along the southwestern margin (East Sayan–Tunka area), and more extensional along the southeastern margin (Baikal–Barguzin area). For this reason, the East Sayan area displays a tectonic behaviour which seems more related to the Altai–Sayan province than to the Baikal Rift System itself. The boundary between these two provinces is sharp and corresponds to the Main Sayan fault.

The stress regime evolution during the Cenozoic can be subdivided in two major paleostress stages, each of them displaying stress regime fluctuation in time and space. In particular, our results show (1) the transpressional stress conditions during the initial stage of rift development, (2) the progressive appearance of extensional stress field during the ‘slow rifting’ stage in Central Baikal, (3) a marked change in the stress regime at the beginning of the Late Pliocene, resulting in the onset of the ‘fast rifting’ stage, and (4) the evolution towards a more extensional regime during the ‘fast rifting’ stage in East Sayan.

The presence of strongly compressional stress field and oblique thrusting in East Sayan area during the ‘slow rifting’ stage suggests that the opening of the South Baikal basin is the result of a passive space-accommodation process, controlled by the lateral southeastwards expulsion of the East Sayan block along the southwestern margin of the Angara–Lena Platform. This indicates that the Baikal Rift has been initiated by an extrusion mechanism, due to the interaction of far-field compressional stress on a mechanically heterogeneous crust. The southwards projection of the Siberian Craton was then acting as a passive oblique indenter. During the ‘fast rifting’ stage, rifting seems to be mainly driven by the presence of density anomalies in the lithosphere, but the lateral extrusion mechanism in the southwestern part of the rift system is still operating. The present-day stress field in the Baikal Rift System and surrounding area can be explained by the superposition of extensional stresses, locally generated by the anomalous lithosphere, on a continental-scale compressional stress field.

The timing of relief formation, sedimentation, major volcanic activity and the stress field evolution together suggest that the lithospheric anomalies and

asthenospheric diapirism appear progressively in the course of rifting and are not the cause, but rather the consequence of rifting. Our work shows that both 'active' and 'passive' mechanisms of rifting are involved in the rifting process, but at different stages of the rifting history. Rifting was initiated as a 'passive' mechanism in the Late Oligocene, and the mechanism turns progressively into a 'active' one in the Late Miocene–Early Pliocene.

### Acknowledgements

This work has been realised in the framework of the project CASIMIR (Comparative Analysis of Sedimentary Infill Mechanisms in Rifts), a joint project of the Baikal International Centre for Ecological Research (BICER) at Irkutsk (Russia) and the Royal Museum for Central Africa at Tervuren (Belgium).

We thank the Federal Scientific Institutes of Belgium, the Siberian branch of the Russian Academy of Sciences and INTAS for financial support. We are specially grateful to Academician N.A. Logatchev and Prof. J. Klerkx for promoting this research. K. Theunissen, J. Klerkx and J. Déverchère are also thanked for helpful discussions, and S. Cloetingh for the organisation of the ILP Task Force 'Origin of Sedimentary Basins', to which this paper is contributing. This is a contribution to IGCP400 project 'Geodynamics of Continental Rifting', UMR publication number 92 and NSG Publication 970161. The digitizing of the topographic maps for the DTM was done by A. Dierickx and the drawings by S. Jacobs. Comments by Max Fernandez, C. Matton and critical reviews by L. Ratschbacher and two anonymous reviewers are appreciated.

### Appendix A

Paleostress tensors from fault-slip data. Lat. = latitude N (°, '); Long. = longitude E (°, ');  $n$  = number of fault data used for stress tensor determination (index mentioning to which phase belong the second (or third) set: o = pre rift phase, p = proto rift phase, a = active rift phase);  $n_T$  = total number of fault data measured;  $\sigma_1$ ,  $\sigma_2$  and  $\sigma_3$  = plunge and azimuth of principal stress axes;  $R$  = stress ratio  $(\sigma_2 - \sigma_3)/(\sigma_1 - \sigma_3)$ ;  $\alpha$  = mean slip deviation (°);  $Q$  = quality ranking as defined in Table 1;  $R'$  = tensor type index as defined in text.

#### A.1. Paleostress tensors for the 'proto rift' phase

Site	Lat.	Long.	Description	$n$	$n_T$	$\sigma_1$	$\sigma_2$	$\sigma_3$	$R$	$\alpha$	$Q$	$R'$
<i>Northwest Baikal</i>												
BA078	55 40	109 25	Kichersky fault, on clay gouge	21 <sup>(o)</sup>	49	06/075	82/218	05/344	0.35	8.2	B	1.65
BA220	54 06	108 17	Cagan-Marian, on clay gouge	17	24	21/068	58/300	23/167	0.58	7.8	A	1.42
BA221	54 04	108 17	Cagan-Marian: incohesive fault gouge	15	25	09/036	01/126	81/221	0.12	8.2	B	2.12
Weighed mean: 3 tensors				53		13/060	77.273	07/152	0.29			1.71
<i>Barguzin Range</i>												
BA204	53 52	109 47	Barguzin scarp, upper part (epidote)	20	33	28/101	60/306	11/196	0.31	11.7	B	1.69
BA207	54 42	110 42	Barguzin scarp: Alla River pre-rift scarp	19 <sup>(aa)</sup>	109	08/100	18/192	71/348	0.22	10.6	C	2.22
Weighed mean: 2 tensors				39		18/100	66/322	15/195	0.04			1.96
<i>Sviatoy Nos area</i>												
BA200	53 22	108 58	Barguzin bay (older)	25 <sup>(p)</sup>	119	26/037	29/292	50/161	0.26	12.1	C	2.26
BA200	53 22	108 58	Barguzin bay (younger)	40 <sup>(p)</sup>	119	19/238	64/102	17/334	0.87	9.7	B	1.13
BA215	53 39	109 00	Chivirkuy bay: Manachovo	17	55	55/017	21/254	27/153	0.87	10.1	C	0.87
BA216	53 40	109 07	Chivirkuy bay: island cut by fault	13	18	15/257	71/038	12/164	0.66	8.2	B	1.34
Weighed mean: 4 tensors				95		10/239	79/085	05/330	0.73			1.27
<i>Olkhon – Small Sea area</i>												
BA008	53 09	106 56	Small Sea, Chadorta: on clay gouge	10	14	21/033	10/127	67/240	0.39	14.4	C	2.39
BA012	53 18	107 37	Olkhon Isl., Sasa cape: on clay gouge	6	8	17/021	73/214	03/112	0.08	12.5	C	1.92
BA010	53 15	107 29	Olkhon Island: on clay gouge	6	9	03/031	12/122	77/292	0.59	11.1	C	2.59
BA006	53 01	106 56	Olkhon Gate, Olkhon: on clay gouge	11	17	71/155	10/036	11/303	0.83	15.9	C	0.83

## A.1. Paleostress tensors for the 'proto rift' phase (continued)

Site	Lat.	Long.	Description	<i>n</i>	<i>n<sub>T</sub></i>	$\sigma_1$	$\sigma_2$	$\sigma_3$	<i>R</i>	$\alpha$	<i>Q</i>	<i>R'</i>
BA007	53 01	106 51	Priolkhon, Kurkut bay: on clay gouge	7	8	19/011	10/105	68/222	0.69	11.5	C	2.69
BA051	53 00	106 54	Olkhon Gate, Priolkhon: clay gouge	10	28	18/046	63/174	20/309	0.67	6.9	B	1.33
Weighed mean: 6 tensors				50		16/026	74/205	00/296	0.30			1.70
<i>Sayan – Tunka area</i> (Late Miocene–Early Pliocene)												
BA024	54 45	103 38	Kultuk, East Sayan fault, mylonites	33 <sup>(oa)</sup>	73	09/098	06/007	79/243	0.48	9.6	B	2.48
BA240	51 57	102 20	Tunka Ridge, 11.4 Ma faulted dyke	20	25	31/305	20/203	52/086	0.05	7.3	A	2.05
BA233	51 45	101 02	Khulugaima volc. 16.5 ± 0.8 Ma	22	31	07/107	32/013	58/207	0.49	11.7	B	2.49
Weighed mean: 3 tensors				76		03/288	08/198	80/168	0.37			2.37

## A.2. Paleostress tensors for the 'active rift' phase

Site	Lat.	Long.	Description	<i>n</i>	<i>n<sub>T</sub></i>	$\sigma_1$	$\sigma_2$	$\sigma_3$	<i>R</i>	$\alpha$	<i>Q</i>	<i>R'</i>
<i>North Baikal</i>												
BA078	55 40	109 25	Ceverobaikalsk: Kichersky fault	14 <sup>(p)</sup>	48	61/325	00/235	29/145	0.09	8.7	C	0.09
<i>Barguzin basin</i>												
BA201	53 50	109 54	Barguzin scarp, Uliun village	40	52	74/236	14/026	08/118	0.60	10.2	B	0.60
BA206	55 57	110 04	Barguzin scarp, Tyn River	7	35	62/206	27/030	02/298	0.63	7.7	D	0.63
BA207	54 42	110 42	Barguzin scarp, Alla River (hot springs)	22 <sup>(pa)</sup>	109	60/140	02/234	30/325	0.48	10.6	C	0.48
BA207	54 42	110 42	Barguzin scarp, Alla River (hot springs)	53 <sup>(pa)</sup>	109	80/267	05/028	09/118	0.32	11.9	A	0.32
BA208	55 30	110 29	Barguzin scarp, Chamanta River	19	29	71/188	06/080	18/348	0.36	3.5	A	0.36
Weighed mean: 5 tensors				141		81/200	08/041	03/310	0.45			0.45
<i>Sviatoy Nos area</i>												
BA212	53 49	109 02	Sviatoy Nos Peninsula: N extremity	11	53	60/320	05/222	29/129	0.40	7.1	C	0.40
BA211	53 38	108 40	W side: joints in Late Mio–Pliocene sand	10	11	74/214	16/038	01/308	0.23	7.2	B	0.23
BA210	53 29	108 31	Sviatoy Nos peninsula, S extremity	52 <sup>(o)</sup>	104	68/359	21/193	05/101	0.40	8.7	A	0.40
BA199	53 16	108 48	Barguzin Bay, Maximicha camp	17	25	73/083	12/220	11/312	0.39	9.9	B	0.39
Weighed mean: 4 tensors				90		77/003	12/211	06/119	0.38			0.38
<i>Olkhon – Small Sea area</i>												
BA071	54 00	108 12	Cape Kedrovoy: Baikalsky fault	18 <sup>(o)</sup>	54	81/332	05/210	07/119	0.28	14	C	0.28
BA013	53 14	107 34	Small Sea, Kulgana: Primorsky fault	16	24	75/063	14/216	06/307	0.18	8.7	A	0.18
BA014	53 07	106 48	Sarma River: Primorsky fault scarp	49 <sup>(o)</sup>	67	72/347	02/249	18/158	0.26	8.5	A	0.26
BA063	53 07	106 49	Sarma River: Primorsky fault scarp	34	38	81/327	00/232	09/142	0.18	8.4	A	0.18
BA064	53 07	106 50	Sarma River: Primorsky fault scarp	37	38	86/103	03/242	03/332	0.21	8.5	A	0.21
BA069	53 24	107 46	N. Olkhon Isl.: Academician ridge	23	41	72/124	03/024	18/294	0.08	12.4	A	0.08
BA070	53 24	107 47	N. Olkhon Isl.: Academician ridge	17 <sup>(p)</sup>	35	69/095	13/221	16/315	0.42	11.3	B	0.42
Weighed mean: 7 tensors				196		84/050	06/230	00/140	0.22			0.22
<i>South Baikal</i> (except Holocene)												
BA102	51 49	104 45	Old railway, Sharyzhalgay complex	10 <sup>(o)</sup>	40	61/172	05/273	29/005	0.44		D	0.44
BA108	51 33	105 05	Tankhoi, conj. joints in Miocene sand	31	31	67/015	23/201	02/110	0.37	4.6	B	0.37
Weighed mean: 2 tensors				41					0.38			0.38
<i>Transbaikal</i> (Ulan-Ude area)												
BA109	51 46	107 30	Selenga bridge: incohesive breccia	5 <sup>(o)</sup>	22	20/037	66/250	12/132	0.00	0.4	D	2.00
BA112	51 04	107 48	Tugnui basin: active border fault	7 <sup>(o)</sup>	41	10/198	52/096	36/294	0.52	5.8	D	1.48
Weighed mean: 2 tensors				12		05/027	79/144	10/296	0.30			1.70

## A.2. Paleostress tensors for the 'active rift' phase (continued)

Site	Lat.	Long.	Description	<i>n</i>	<i>nT</i>	$\sigma_1$	$\sigma_2$	$\sigma_3$	<i>R</i>	$\alpha$	<i>Q</i>	<i>R'</i>
<i>Sayan–Tunka</i> (Late Pliocene–middle Pleistocene)												
BA229			Upper Irkut River, PreC. marbles	6	8	05/041	85/243	02/131	0.50	12.1	C	1.50
BA222	51 42	100 57	Mondy, E.-M. Pliocene conglomerate	62	70	01/246	63/155	26/337	0.07	7.6	A	1.93
BA223	51 39 49	101 40 27	Nilova Putsy, L. Miocene basalt	24 <sup>(p)</sup>	59	15/229	75/047	00/139	0.12	10.3	B	1.88
BA244	51 45 03	103 25 18	Bistraya, E.-M. Plio. conglom. covered by undeformed L. Pleistocene terrace	37	40	17/072	72/226	07/339	0.44	17.0	A	1.56
BA024	54 44 43	103 38 27	Kultuk, Main Sayan Fault, mylonites	18 <sup>(op)</sup>	73	36/073	53/245	04/340	0.13	9.9	C	1.87
Weighed mean: 5 tensors				147		05/061	80/179	09/330	0.19			1.81
<i>South Baikal–Tunka</i> (Late Pleistocene–Holocene)												
BA125	52 18	107 45	Selenga delta: joints in 1862 e.q. scarp	54	72	87/225	02/093	02/003	0.46	17.6	B	0.46
BA242	51 54	102 22	Arshan: joints in Holocene fault scarp	22	25	60/062	30/245	01/154	0.26	7.5	B	0.26
BA236	51 40 18	101 44 26	Turan, L. Pleistocene sand quarry	21	25	85/266	05/072	02/162	0.77	10.2	B	0.77
BA223	51 39 49	101 40 27	Nilova Putsy, L. Miocene basalt	22	59	74/042	08/283	14/191	0.81	12.8	B	0.81
BA230	51 42 11	100 57 32	U. Pleistocene glacial moraine	12	19	81/153	05/023	07/293	0.91	13.1	B	0.91
Weighed mean (Tunka): 4 tensors				77					0.65	0.65		
Arshan–Turan (BA242 + BA236):				43		77/057	13/248	02/158	0.51	0.51		

## Appendix B

Local and regional fault kinematics, based on slip calculations from the mean movement planes and the related stress tensor, using the method of Means (1989). The separation of the total fault population into subsets, for the determination of the mean movement planes, is based on the technique of Huang and Charlesworth (1989).

## B.1. Fault kinematics for the 'proto rift' phase

Site	Structure	<i>n</i>	Rank	Principal movement plane	Auxiliary movement plane
<i>North Baikal</i>					
BA078	Kichersky fault	21	B	11 × 67/317 12/042 ND	9 × 74/281 08/193 ID
<i>Northwest Baikal</i>					
BA220	Baikalsky fault	21	A	17 × 60/008 00/098 IS	4 × 78/130 21/215 ND
BA221	Baikalsky fault	15	B	6 × 85/249 10/338 ND	5 × 49/021 46/045 IS
<i>Barguzin Range</i>					
BA204	Barguzin fault	20	B	7 × 77/009 23/093 ND	6 × 71/294 26/014 ND
BA207	Barguzin fault	19	C	11 × 44/266 21/292 IS	5 × 86/076 28/164 IS
<i>Sviatoy Nos area</i>					
BA200	Barguzin bay (1)	25	C	17 × 60/008 48/059 IS	4 × 78/130 63/064 NS
BA200	Barguzin bay (2)	40	B	30 × 79/349 56/276 NS	6 × 89/292 20/022 ND
BA215	Chivirkuy Bay	17	C	7 × 85/354 53/077 IS	5 × 80/124 57/198 ND
BA216	Chivirkuy Bay	13	B	10 × 74/025 02/296 NS	3 × 76/346 34/266 NS
<i>Olkhon – Small Sea area</i>					
BA008	Primorsky/Small Sea	10	C	8 × 68/155 08/242 IS	2 × 48/339 48/331 ID
BA012	Olkhon/Small Sea	6	C	6 × 51/271 06/357 ND	
BA010	Olkhon/Small Sea	6	C	3 × 76/094 54/024 ID	2 × 75/310 30/031 IS
BA006	Olkhon Gate	11	C	7 × 89/342 32/253 NS	2 × 49/065 14/143 ND
BA007	Olkhon Gate	7	C	5 × 63/137 36/205 IS	2 × 56/266 37/207 ID
BA051	Olkhon Gate	10	B	8 × 64/347 28/272 NS	
Mean movement vector for Northwest Baikal, Barguzin, Sviatoy Nos and Olkhon–Small Sea					
transpressive substage				46 × 18/044 IS;	
transtensive substage				96 × 18/281 NS	

## B.1. Fault kinematics for the 'proto rift' phase (continued)

Site	Structure	<i>n</i>	Rank	Principal movement plane	Auxiliary movement plane
<i>Sayan–Tunka area</i>					
BA024	Main Sayan fault	33	B	14 × 48/283 45/266 ID	9 × 86/234 21/146 NS
BA240	Tunka Ridge, dyke	20	A	14 × 54/194 11/276 ND	3 × 13/324 12/303 NS
BA233	Tunka fault	22	B	19 × 50/337 29 271 ID	2 × 87/238 34/150 NS
Mean movement vector for Sayan–Tunka				57 × 28/269 ID	

## B.2. Fault kinematics for the 'active rift' phase

Site	Structure	<i>n</i>	Rank	Principal movement plane	Auxiliary movement plane
<i>North Baikal</i>					
BA078	Kichersky fault	14	C	7 × 81/329 81/323 NS	
<i>Barguzin basin</i>					
BA201-3	Barguzin fault	16	B	25 × 62/141 58/109 NS	9 × 47/311 42/282 NS
BA206	Barguzin fault	7	D	7 × 73/139 39/063 NS	
BA207	Barguzin fault	22	C	13 × 85/331 85/321 NS	4 × 65/027 60/062 ND.
BA207	Barguzin fault	53	A	30 × 67/166 67/125 NS	
BA208	Barguzin fault	19	A	10 × 79/351 77/322 NS	
Weighed mean: 5 tensors		117		69 × 64/143 62/122 NS (Barguzin fault: pure normal) 35 × 66/321 66/288 N (conjugated system) 15 × 73/030 69/352 NS (transversal faults)	
<i>Sviatoy Nos area</i>					
BA212	Sviatoy Nos, N. point	11	C	6 × 43/314 43/309 NS	
BA211	Sviatoy Nos, W side	10	B	6 × 67/315 62/277 NS	4 × 76/123 68/176 ND
BA210	Sviatoy Nos, S. point	52	A	29 × 63/130 50/077 NS	
BA199	Barguzin Bay	17	B	9 × 66/292 30/332 ND	
Weighed mean: 11 tensors		90		37 × 64/130 60/098 NS (NW side of Sviatoy Peninsula) 36 × 56/297 55/314 ND (SE side + Barguzin Bay)	
<i>Olkhon – Small Sea area</i>					
BA071	Baikalsky fault	18	C	9 × 63/142 61/117 NS	
BA013	Primorsky fault	16	A	8 × 60/315 58/337 ND	
BA014	Primorsky fault	49	A	27 × 56/154 56/148 NS	
BA063	Primorsky fault	34	A	24 × 70/141 70/140 NS	
BA064	Primorsky fault	37	A	24 × 49/149 49/146 NS	
BA069	Olkhon, Akad. Ridge	23	A	14 × 60/308 60/309 ND	
BA070	Olkhon, Akad. Ridge	17	B	12 × 75/358 63/300 NS	
Weighed mean: 7 tensors		194		99 × 62/149 61/130 NS (Primorsky fault: pure normal) 51 × 65/326 65/331 N (conjugated system) 18 × 88/067 38/339 ID (transversal faults: oblique)	
<i>Sayan–Tunka (Late Pliocene–middle Pleistocene)</i>					
BA222	South Tunka fault	62	A	28 × 88/173 07/263 IS	
BA223	South Tunka fault	24	B	18 × 88/179 18/268 IS	
BA244	South Tunka fault	37	A	13 × 43/220 12/297 IS	
BA024	Main Sayan Fault	18	C	10 × 82/234 55/156 NS	
Weighed mean: 5 tensors		141		51 × 83/174 01/084 NS (South Tunka fault: left-lateral) 31 × 83/307 09/036 ND (Tunka basin: south-border fault) 22 × 45/214 29/271 IS (associated thrust) 15 × 89/056 45/145 IS (Main Sayan fault: oblique sinistral)	

## B.2. Fault kinematics for the 'active rift' phase (continued)

Site	Structure	<i>n</i>	Rank	Principal movement plane	Auxiliary movement plane
<i>South Baikal (except Holocene)</i>					
BA102	Sharyzhalgay	10	D	6 × 80/000 01/354 ND	
BA108	Miocene sands	31	A	5 × 87/327 30/055 IS	2 × 67/344 22/264 NS
<i>Transbaikal (Ulan-Ude area)</i>					
BA109	Selenga bridge	5	D	5 × 88/341 23/070 IS	
BA112	Tugnui basin	7	D	7 × 71/188 48/255 IS	
<i>South Baikal–Tunka (Late Pleistocene–Holocene)</i>					
BA125	Selenga delta	65	B	25 × 86/227 04/137 NS	15 × 66/182 66/188 ND 12 × 69/007 68/351NS
BA242	Tunka fault, Arshan	22	B	18 × 66/178 47/117 NS	4 × 71/321 52/025 ND
BA236	Tunka fault, Turan	21	B	12 × 85/186 18/098 NS	9 × 76/311 24/035 ND
BA223	Tunka fault, Nilova	22	B	17 × 60/175 57/203 ND	3 × 74/027 06/299 NS
BA230	Tunka fault, Mondy	12	B	11 × 80/348 18/261 NS	
Arshan–Turan (BA242 + 236)		43		24 × 68/173 58/124 NS	13 × 74/314 46/027 ND 6 × 85/030 11/119 IS]

## References

- Agar, S.M., Klitgord, K.D., 1995. Rift flank segmentation, basin initiation and propagation: a neotectonic example from Lake Baikal. *J. Geol. Soc.*, London 152, 849–860.
- Angelier, J., 1991. Inversion directe de recherche 4-D: comparaison physique et mathématique de deux méthodes de détermination des tenseurs des paléocontraintes en tectonique de failles. *C.R. Acad. Sci.*, Paris 312 (II), 1213–1218.
- Angelier, J., 1994. Fault slip analysis and paleostress reconstruction. In: Hancock, P.L. (Ed.) *Continental Deformation*. Pergamon, Oxford, pp. 101–120.
- Angelier, J., Mechler, P., 1977. Sur une méthode graphique de recherche des contraintes principales également utilisable en tectonique et en sismologie: la méthode des dièdres droits. *Bull. Soc. Géol. Fr.* 7 (19), 1309–1318.
- Artyushkov, E.V., Letnikov, F.A., Ruzhich, V.D., 1990. The mechanism of formation of the Baikal rift basin. *J. Geodyn.* 11, 277–291.
- Bagdasaryan, G.P., Geracimobskiy, B.I., Polyakov, A.I., Gukasyan, R.Kh., 1981. New data on absolute age and chemical composition of volcanics from the Baikal Rift System (in Russian). *Geochimiya*, 3: 342–350.
- Baljinnyam, I., Bayasgalan, A., Borisov, B.A., Cisternas, A., Dem'yanovich, M.G., Ganbaatar, L., Kochetkov, V.M., Kurushin, R.A., Molnar, P., Philip, H., Vashchilov, Y.Y., 1993. Ruptures of major earthquakes and active deformation in Mongolia and its surroundings. *Geol. Soc. Am.*, Mem. 181, 62 pp.
- Balla, Z., Kuzmin, M., Levi, K., 1991. Kinematics of the Baikal opening: results of modeling. *Ann. Tectonicae* 5 (1), 18–31.
- Bogdanov, Y.A., Zonenshain, L.P., 1991. Exposures of Miocene sediments at the bottom of Lake Baikal and the dating of lake-bottom faulting on the basis of their observation from Pisces submersibles. *Trans. Acad. Sci. USSR, Earth Sci.* 321 (8), 122–125.
- Bott, M.H.P., 1959. The mechanisms of oblique slip faulting. *Geol. Mag.* 96, 109–117.
- Braun, J., Beaumont, C., 1989. A physical explanation of the relation between the rift flank uplifts and the breakup unconformity at rifted continental margins. *Geology* 17, 760–764.
- Burov, E.B., Houdry, F., Diament, M., Déverchère, J., 1994. A broken plate beneath the North Baikal Rift System revealed by gravity modelling. *Geophys. Res. Lett.* 21, 129–132.
- Carey-Gailhardis, E., Mercier, J.-L., 1987. A numerical method for determining the state of stress using focal mechanisms of earthquake populations: application to Tibetan teleseisms and microseismicity of southern Peru. *Earth. Planet. Sci. Lett.* 82, 165–179.
- Cloetingh, S., Kooi, H., 1992. Intraplate stresses and dynamical aspects of rift basins. *Tectonophysics* 215, 167–185.
- Cobbold, P.R., Davy, P., 1988. Indentation tectonics in nature and experiment, 2. Central Asia. *Bull. Geol. Inst. Uppsala, N.S.*, 14: 143–162.
- Delvaux, D., 1993. The TENSOR program for reconstruction: examples from the east African and the Baikal Rift Systems. *Terra Abstr.*, Abstr. suppl. Terra Nova, 5: 216.
- Delvaux, D., Klerkx, J., 1994. Baikal rifting mechanism: from passive to active? *Eos, Trans. Am. Geophys. Union*, 75 (44): 599.
- Delvaux, D., Moeys, R., Stapel, G., Melnikov, A., Ermikov, V., 1995. Paleostress reconstructions and geodynamics of the Baikal region, Central Asia. Part I. Paleozoic and Mesozoic pre-rift evolution. In: Cloetingh, S., D'Argenio, B., Catalano, R., Horvath, H., Sassi, W. (Eds.), *Interplay of Extension and Compression in Basin Formation*. *Tectonophysics*, 252: 61–101.
- Déverchère, J., Houdry, F., Solonenko, N.V., Solonenko, A.V., San'kov, V.A., 1993. Seismicity, active faults and stress field

- of the North Muya region, Baikal rift: new insights on the rheology of extended continental lithosphere. *J. Geophys. Res.* 98 (B11), 19895–19912.
- Devyatkin, E.V., 1975. Neotectonic structures of western Mongolia. In: *Mesozoic and Cenozoic Tectonics and Magmatism of Mongolia* (in Russian). Nauka, Moscow, pp. 264–282.
- Devyatkin, E.V., 1981. *The Cenozoic of Inner Asia* (in Russian). Nauka, Moscow, 196 pp.
- Diament, M., Kogan, M.G., 1990. Long wavelength gravity anomalies over the Baikal rift and geodynamic implications. *Geophys. Res. Lett.* 17 (11), 1977–1980.
- Doser, D.I., 1991a. Faulting within the western Baikal rift as characterized by earthquake studies. *Tectonophysics* 196, 87–107.
- Doser, D.I., 1991b. Faulting within the eastern Baikal rift as characterized by earthquake studies. *Tectonophysics* 196, 109–139.
- Dunne, W.M., Hancock, P.L., 1994. Paleostress analysis of small-scale brittle structures. In: Hancock, P.L. (Ed.), *Continental Deformation*. Pergamon, Oxford, pp. 101–120.
- Dupin, J.-M., Sassi, W., Angelier, J., 1993. Homogeneous stress hypothesis and actual fault slip: a distinct element analysis. *J. Struct. Geol.* 15, 1033–1043.
- Engelder, T., 1993. *Stress Regimes in the Lithosphere*. Princeton University Press, Princeton, 457 pp.
- Ermikov, V.D., 1994. Mesozoic precursors of rift structures of Central Asia. *Bull. Centr. Rech. Explor. Prod. Elf Aquitaine* 18 (1), 99–122.
- Eudrichinsky, A.S., 1991. Late Cretaceous and Palaeogene of Trans-Baikal. *Izv. Akad. Nauk USSR* 3, 17–25.
- Gao, S., Davis, P.M., Liu, H., Slack, P.D., Zorin, Y.A., Logatchev, N.A., Kogan, M., Burkholder, P.D., Meyer, R.P., 1994a. Asymmetric upwarp of the asthenosphere beneath the Baikal Rift System, Siberia. *J. Geophys. Res.* 99 (B8), 15319–15330.
- Gao, S., Davis, P.M., Liu, H., Slack, P.D., Zorin, Y.A., Mordvinova, V.V., Kozhevnikov, V.M., Meyer, R.P., 1994b. Seismic anisotropy and mantle flow beneath the Baikal Rift System. *Nature* 371, 149–150.
- Guiraud, M., Laborde, O., Philip, H., 1989. Characterization of various types of deformation and their corresponding deviatoric stress tensor using microfault analysis. *Tectonophysics* 170, 289–316.
- Houdry, F., 1994. Mécanismes de l'extension continentale dans le rift nord-baikal, Sibérie: Contraintes des données d'imagerie SPOT, de terrain, de sismologie et de gravimétrie. Thèse de doctorat de l'Université Pierre et Marie Curie, Paris 6, 345 pp.
- Houdry, F., Déverchère, J., Gaudemer, Y., Burov, E.B., San'kov, V.A., 1994. Evidence for oblique extension in the Baikal Rift, Siberia, from multisource data. *Eos, Trans. Am. Geophys. Union* 75 (44), 599.
- Huang, G., Charlesworth, H., 1989. A FORTRAN-77 program to separate a heterogeneous set of orientations into subsets. *Comput. Geosci.* 15, 1–7.
- Hutchinson, D.R., Golmshtok, A.J., Zonenshain, L.P., Moore, T.C., Scholz, C.A., Klitgord, K.D., 1992. Deposition and tectonic framework of the rift basins of Lake Baikal from multichannel seismic data. *Geology* 20, 589–592.
- Kashik, S.A., Mazilov, V.N., 1994. Main stages and paleogeography of the Cenozoic sedimentation in the Baikal Rift System, Central Asia. *Bull. Centr. Rech. Explor. Prod. Elf Aquitaine* 18 (2), 453–462.
- Kazmin, V.G., Golmshtok, A.Ya., Klitgord, K., Moore, T., Hutchinson, D., Scholz, C., Weber, E., 1995. Structure and development of the Akademicheskii Ridge area (Baikal rift) according to data of seismic and underwater studies. *Russ. Geol. Geophys.* 36 (10), 164–176.
- Kesselman, S.I., Kotliar, P.E., Kuchai, O.A., Tychkov, S.A., Sebrebriakova, L.I., 1992. Deformation of the near-surface part of the Earth's crust by seismologic and geodetic data obtained on Baikal geodynamic polygons. *Tectonophysics* 202, 251–256.
- Kieslev, A.I., Popov, A.M., 1992. Asthenospheric diapir beneath the Baikal rift: petrological constraints. *Tectonophysics* 208, 287–295.
- Kooi, H., Cloetingh, S., 1992. Lithospheric necking and regional isostasy at extensional basins, 2. Stress-induced vertical motions and relative sea level changes. *J. Geophys. Res.* 97 (B12), 17573–17591.
- Kotel'nikov, D.D., Solodkova, N.A., Dombrovskaya, Zh.V., 1993. Clay minerals in surface and buried weathering crusts in the south of the Siberian Platform. *Trans. Acad. Sci. USSR, Earth Sci.* 332 (7), 56–61.
- Levi, K.G., Sherman, S.I., Plyusnina, L.V., 1982. Map of neotectonics of the Baikal and Transbaikal territories. N.A. Logatchev, Editor, Nauka, Institute of the Earth's Crust, Irkutsk.
- Levi, K.G., Miroshnichenko, A.I., San'kov, V.A., Babushkin, S.M., Larkin, G.V., Badardinov, A.A., Wong, H.K., Coleman, S., Delvaux, D., 1998. Active faults of the Baikal Basin. *Bull. Centr. Rech. Explor. Prod. Elf Aquitaine*, 22 (in press).
- Logatchev, N.A., 1993. History and geodynamics of the Baikal rift (east Siberia): a review. *Bull. Centr. Rech. Explor. Prod. Elf Aquitaine* 17 (2), 353–370.
- Logatchev, N.A., Florensov, N.A., 1978. The Baikal system of rift valleys. *Tectonophysics* 45, 1–13.
- Logatchev, N.A., Zorin, Yu.A., 1987. Evidence and cause of the two-stage development of the Baikal rift. *Tectonophysics* 143, 225–234.
- Logatchev, N.A., Zorin, Yu.A., 1992. Baikal Rift System: structure and geodynamics. *Tectonophysics* 208, 273–286.
- Lukina, N.V., 1988. The Baikal intracontinental rift system. In: Kropotkin (Ed.), *Neotectonics and Recent Geodynamics of Mountain belts*. Nauka, Moscow, Transaction 427, 364 pp.
- Mats, V.D., 1993. The structure and evolution of the Baikal rift depression. *Earth Sci. Rev.* 34, 81–118.
- Mazilov, V.N., Kashik, S.A., Lomonosova, T.K., 1993. Oligocene deposits of the Tunka depression (Baikal Rift System). *Russ. Geol. Geophys.* 34 (8), 68–73.
- McCalpin, J.P., Khromovskikh, V.S., 1995. Holocene paleoseismicity of the Tunka fault, Baikal rift, Russia. *Tectonics* 14 (3), 594–605.
- Means, W.D., 1989. A construction for shear stress on a generally oriented plane. *J. Struct. Geol.* 11, 625–627.

- Melnikov, A.I., Mazukabzov, A.M., Sklyarov, E.V., Vasiliev, E.P., 1994. Baikal rift basement: structure and tectonic evolution. *Bull. Centr. Rech. Explor. Prod. Elf Aquitaine* 18 (1), 99–122.
- Molnar, P., Tapponnier, P., 1975. Cenozoic tectonics of Asia: effects of a continental collision. *Science* 189 (4201), 419–426.
- Morley, C.K., Nelson, T.L., Patton, T.L., Muss, S.G., 1990. Transfer zones in the East African rift system. *Am. Assoc. Pet. Geol. Bull.* 74, 1234–1253.
- Nikolaev, P.N., 1977. Technique of stress analysis (in Russian). *Izv. Vuzov Geol. Razvedka* 12, 70–84.
- Nikolaev, V., 1990. Cenozoic history of Baikal depression. *Geotectonica Metallogenia* 14 (4), 339–350.
- Parfënoy, L.M., Koz'min, B.M., Imayev, V.S., Savostin, L.A., 1987. The tectonic character of the Olëkma–Stanovoy seismic zone. *Geotectonics* 21 (6), 560–572.
- Patriat, P., Achache, P., 1984. India–Eurasia collision chronology has implications for crustal shortening and driving mechanism of plates. *Nature* 311, 615–621.
- Petit, C., Déverchère, J., 1995. Velocity structure of the northern Baikal rift, Siberia, from local and regional earthquake travel times. *Geophys. Res. Lett.* 20, 1677–1680.
- Petit, C., Déverchère, J., Houdry-Lémont, F., San'kov, V.A., Melnikova, V.I., Delvaux, D., 1996. Present-day stress field changes along the Baikal rift and tectonic implications. *Tectonics* 15 (6), 1171–1191.
- Pollard, D.D., Saltzer, S.D., Rubin, A., 1993. Stress inversion methods: are they based on faulty assumptions?. *J. Struct. Geol.* 15 (8), 1045–1054.
- Popova, S.M., Mats, V.D., Chernayeva, M.K., 1989. Paleolimnological reconstructions. The Baikal Rift System (in Russian). Nauka, Novosibirsk, 111 pp.
- Rasskazov, S.V., 1985. Basalts of the Udokan field, Baikal Rift System (in Russian). Nauka, Novosibirsk, 141 pp.
- Rasskazov, S.V., 1990. The Pliocene–Quaternary thrust fault in the south of the Oka Plateau, Eastern Sayan Mountains. *Russ. Geol. Geophys.* 31 (5), 134–138.
- Rasskazov, S.V., 1993. Magmatism of the Baikal Rift System (in Russian). Nauka, Novosibirsk, 285 pp.
- Rasskazov, S.V., 1994. Rift-related magmatism and geodynamics south of the Siberian Craton. *Bull. Centr. Rech. Explor. Prod. Elf Aquitaine*. 18 (2), 437–452.
- Richardson, R.M., 1992. Ridge forces, absolute plate motions and the intraplate stress field. *J. Geophys. Res.* 97 (B8), 11739–11748.
- Ruppel, C.D., Kogan, M.G., McNutt, M.K., 1993. Implications of new gravity data for Baikal rift structure. *Geophys. Res. Lett.* 20, 1635–1638.
- Ruzhich, V.V., Sherman, S.I., Tarasevitch, S.I., 1972. New data on thrust faults in the southwestern Baikal Rift System. *Trans. Acad. Sci. USSR, Earth Sci.* 205 (1–6), 68–71.
- San'kov, V.A., Dneprovskii, Yu.I., Kovalenko, S.N. et al., 1991. Faults and Seismicity of the North-Muya Geodynamic Polygon (in Russian). Nauka Novosibirsk.
- Scholz, C.A., Klitgord, K.D., Hutchinson, D.R., Ten Brink, U.S., Zonenshain, L.P., Golmshtok, A.Y., Moore, T.C., 1993. Results of 1992 seismic reflection experiment in Lake Baikal. *Eos, Trans. Am. Geophys. Union* 74, 465–470.
- Sherman, S.I., 1992. Faults and tectonic stresses of the Baikal Rift System. *Tectonophysics* 208, 297–307.
- Sherman, S.I., Dneprovskii, Yu.I., 1989. Stress Fields of the Earth's Crust and Geostructural Methods of Their Investigations (in Russian). Nauka, Novosibirsk, 157 pp.
- Sherman, S.I., Ruzhich, V.V., 1973. Folds and faults of the basement. West Pribaikalia, Khamar–Daban and North Mongolia. In: *Tectonics and Volcanism of the Southwest Part of the Baikal Rift System* (in Russian). Nauka, Moscow, pp. 24–35.
- Sherman, S.I., Levi, K., Ruzhich, V.V., San'kov, V.A., Dneprovskiy, J.J., Rasskazov, S.V., 1984. Geology and seismicity of the Baikal–Amur railway. In: Logatchev, N.A. (Ed.), *Neotectonics* (in Russian). Nauka, Novosibirsk, 206 pp.
- Solonenko, A.V., 1993. Symmetry of the crustal stress field in the Baikal Rift Zone. *Trans. Acad. Sci. USSR, Earth Sci.* 330 (4), 53–57.
- Solonenko, A.V., Solonenko, N.V., Melnikova, V.I., Shteiman, E.A., 1997. The seismicity and earthquake focal mechanisms of the Baikal seismic zone. *Bull. Centr. Rech. Explor. Prod. Elf Aquitaine* 21 (in press).
- Sonder, L.J., 1990. Effects of density contrasts on the orientation of stresses in the lithosphere: relation to principal stress directions in the Transverse ranges, California. *Tectonics* 9, 761–771.
- Tapponnier, P., Molnar, P., 1979. Active faulting and Cenozoic tectonics of the Tian Shan, Mongolia and Baikal regions. *J. Geophys. Res.* 84 (B7), 3425–3459.
- Timofeev, V.Y., Panin, S.F., Sarycheva, Y.K., Anisimova, L.V., Gridnev, D.G., Masalskii, O.K., 1994. Investigation of earth surface tilts and strains in the Baikal Rift System (Talaya station). *Russ. Geol. Geophys.* 35 (3), 101–110.
- Ufimtsev, G.F., 1991. Morphotectonics of the Baikal Rift Valley, Eastern Siberia, USSR. *Geojournal* 23 (3), 197–206.
- Van der Beeck, P.A., 1997. Flank uplift and topography at the Central Baikal Rift (SE Siberia): a test of kinematic models for continental extension. *Tectonics* 16, 122–136.
- Van der Beek, P.A., Delvaux, D., Andriessen, P.A.M., Levi, K.G., 1996. Early Cretaceous denudation related to convergent tectonics in the Baikal region, SE Siberia. *J. Geol. Soc. London* 153, 515–523.
- Windley, F.F., Allen, M.B., 1993. Mongolian plateau: evidence for a late Cenozoic mantle under Central Asia. *Geology* 21, 295–298.
- Worral, D.M., Kruglyak, V., Kunst, F., Kuznetsov, V., 1996. Tertiary tectonics of the Sea of Okhotsk, Russia: far-field effects of the India–Eurasia collision. *Tectonics* 15, 813–826.
- Zamaraev, S.M., Ruzhich, V.V., 1978. On relationships between the Baikal rift and ancient structures. In: Logatchev, N.A., Mohr, P.A. (Eds.), *Geodynamics of the Baikal Rift System*. *Tectonophysics* 45, 41–47.
- Zhonghuai, X., Suyun, W., Yuri, H., Ajia, G., 1992. Tectonic stress of China inferred from a large number of small earthquake. *J. Geophys. Res.* 97, 11867–11877.
- Ziegler, P.A., 1996. Geodynamic processes governing development of rifted basins. In: Roure, F., Ellouz, N., Shein, V.S.,

- Skvortsov, I. (Eds.), *Geodynamic Evolution of Sedimentary Basins*. Technip, Paris, pp. 19–67.
- Zoback, M.L., 1992. First- and second-order patterns of stress in the lithosphere: the World Stress Map Project. *J. Geophys. Res.* 97, 11703–11728.
- Zoback, M.D., Stephenson, R.A., Cloetingh, S., Larsen, B.T., Van Hoorn, B., Robinson, A., Horvath, F., Puigdefabregas, C., Ben-Avraham, Z., 1993. Stresses in the lithosphere and sedimentary basin evolution. *Tectonophysics* 226, 1–13.
- Zonenshain, L.P., Savostin, L.A., 1981. Geodynamics of the Baikal Rift System and plate tectonics of Asia. *Tectonophysics* 76 (1-2), 1–45.
- Zonenshain, L.P., Kazmin, V.V., Kuzmin, M.M., Dobretsov, N.L., Baranov, B.V., Kononov, M.V., Mats, V.D., Balla, Z., Fialkov, V.A., Kharchenko, V.V., 1993. Geology of the floor of Lake Kaikal: Data obtained with the PISCES manned submersibles. *Trans. Acad. Sci. USSR, Earth Sci.* 331A (6), 55–61.
- Zorin, Yu.A., Kozhevnikov, V.M., Novoselova, M.R., Turutanov, E.K., 1989. Thickness of the lithosphere beneath the Baikal Rift System and adjacent regions. *Tectonophysics* 168, 327–337.